

1 Introducing new lightning schemes into the CHASER (MIROC) 2 chemistry climate model

3 Yanfeng He¹, Hossain Mohammed Syedul Hoque¹, Kengo Sudo^{1,2}

4 ¹ Graduate School of Environment Studies, Nagoya University, Nagoya, 464-8601, Japan

5 ² Japan Agency for Marine–Earth Science and Technology (JAMSTEC), 237-0061, Yokohama, Japan

6 Correspondence to: Yanfeng He (hyf412694462@gmail.com)

7 **Abstract.** The formation of nitrogen oxides (NO_x) associated with lightning activities (hereinafter designated as LNO_x) is a
8 major source of NO_x. In fact, it is regarded as the ~~most~~-dominant NO_x source in the middle to upper troposphere. Therefore,
9 ~~improve~~improving the prediction accuracy of lightning and LNO_x in chemical climate models is crucially important. This
10 study implemented ~~two~~three new lightning schemes with the CHASER (MIROC) global chemical transport/climate model.
11 The first lightning scheme is based on upward cloud ice flux (ICEFLUX scheme), ~~whereas the~~. The second, one (the original
12 ECMWF scheme), also adopted in the European Centre for Medium-Range Weather Forecasts (ECMWF) forecasting system
13 ~~(original ECMWF scheme)~~. In, calculates lightning flash rates as a function of Q_R (a quantity intended to represent the ease
14 of charging rate of collisions between graupel and other types of hydrometeors inside the charge separation region), convective
15 available potential energy (CAPE), and convective cloud-base height. For the original ECMWF scheme, by tuning the
16 equations and adjustment factors for land and ocean, a ~~modified~~new lightning scheme named ECMWF-McCAUL scheme was
17 also tested in CHASER. The ECMWF-McCAUL scheme calculates lightning flash rates as a function of CAPE and column
18 precipitating ice. In the original version of CHASER (MIROC), lightning is initially parameterized with the widely used cloud
19 top height scheme (CTH scheme). Model evaluations with lightning observations conducted using ~~an optical transient~~
20 ~~detector~~the Lightning Imaging Sensor (LIS) and Optical Transient Detector (OTD) indicate that both the ICEFLUX and
21 ECMWF schemes simulate the spatial distribution of lightning more accurately on a global scale than the CTH scheme does.
22 The ~~modified~~-ECMWF-McCAUL scheme showed the highest prediction accuracy for the global distribution of lightning.
23 ValidationEvaluation by atmospheric tomography (ATom) aircraft observations (NO) and tropospheric monitoring instrument
24 (TROPOMI) satellite observations (NO₂) shows that the ~~ICEFLUX scheme reduced~~newly implemented lightning schemes
25 partially facilitated the reduction of model biases to a greater extent than(NO and NO₂) typically within the ECMWF
26 schemesregions where LNO_x is the major source of NO_x when compared using ~~the~~-CTH scheme. ~~The effects of the newly~~
27 ~~introduced lightning schemes on the tropospheric chemical fields were evaluated by comparison with~~ the CTH scheme.
28 Although the newly implemented lightning schemes have a minor effect on the tropospheric mean oxidation capacity compared
29 to the CTH scheme, they led to marked changechanges of oxidation capacity in different regions of the troposphere. ~~Long-~~
30 ~~term~~Historical trend analyses of flash and surface temperatures predicted using CHASER (2001–2020) show that lightning
31 schemes predicted an increasing trend of lightning or no significant trends, except for one case of the ICEFLUX scheme,
32 which predicted a decreasing trend of lightning. The global lightning rates of increase during 2001–2020 predicted by the
33 CTH scheme were 17.~~86~~69%/°C and 2.~~60~~50%/°C, respectively, with and without meteorological nudging, ~~which are slightly~~
34 ~~beyond~~. The un-nudged runs also included the rangeshort-term surface warming but without the application of ~~an earlier study~~
35 ~~(5%/°C–16%/°C)~~meteorological nudging. Furthermore, the ECMWF schemes predicted a larger increasing trend of lightning
36 flash rates under globalthe short-term surface warming by a factor of ~~3~~ (~~modified~~-4 (ECMWF-McCAUL scheme) and 5
37 (original ECMWF scheme) compared to the CTH scheme without nudging. In conclusion, the ~~two~~three new lightning schemes
38 improved global lightning prediction in the CHASER model. However, further research is needed to assess the
39 ~~reproductivity~~reproducibility of ~~long-term~~-trends of lightning over longer periods.

40 **Keywords**

41 lightning, lightning scheme, lightning NO_x, chemistry-climate model, lightning under climate change

42 **1 Introduction**

43 ~~Reactive nitric~~Nitric oxide (NO) can be formed during lightning activities. Also, NO can be oxidized quickly to nitrogen
44 dioxide (NO₂). An equilibrium between NO and NO₂ can be reached during daytime. Those gases are known collectively as
45 NO_x (Finney ~~et al.~~, 2014). Actually, LNO_x is estimated as contributing approximately 10% of the global NO_x source.
46 Regarded as the ~~most~~ dominant NO_x source in the middle to upper troposphere (Schumann and Huntrieser, 2007; Finney et
47 al., 2016a), NO_x is associated with many chemical reactions in the atmosphere. Most importantly, NO reacts with peroxy
48 radical to reproduce OH radical. Photochemical dissociation of NO₂ engenders the production of ozone (Isaksen and Hov,
49 1987; Grewe, 2007). The primary oxidants in the atmosphere, which are OH radical and ozone, control the oxidation
50 capacity of the atmosphere. Results of several studies have indicated that global-scale LNO_x emissions are an important
51 contributor to ozone and other trace gases, especially in the upper troposphere (Labrador et al., 2005; Wild, 2007; Liaskos et
52 al., 2015). Consequently, LNO_x influences atmospheric chemistry and global climate to a considerable degree (Schumann
53 and Huntrieser, 2007; Murray, 2016; Finney et al., 2016b; Tost, 2017). However, large uncertainties remain in predicting
54 lightning and LNO_x in chemical climate models (Tost et al., 2007). Therefore, improving lightning prediction accuracy and
55 quantifying LNO_x in chemical climate models is crucially important for future atmospheric research.

56

57 ~~Chemical~~Global chemical climate models (CCMs) such as CHASER (MIROC) (Sudo et al., 2002; Sudo and Akimoto, 2007;
58 Watanabe et al., 2011) most often use the convective cloud-top height to parameterize the lightning flash rate (Price and
59 Rind, 1992; Lamarque et al., 2013). ~~However, some new lightning schemes have been devised to simulate better the spatial
60 and temporal correlation and root mean square error (RMSE) compared to the~~The Earth System Models (ESMs) recently
61 used in the sixth Coupled Model Intercomparison Project (CMIP6) all used the convective cloud-top height to calculate the
62 lightning flash rates (Thornhill et al., 2021). Not only in global CCMs but the studies of LNO_x in regional-scale models have
63 also made significant progress in recent years (Heath et al., 2016; Kang et al., 2019a; Kang et al., 2019b; Kang et al., 2020).

64

65 The spaceborne Lightning Imaging Sensor (LIS) and Optical Transient Detector (OTD) lightning observation data
66 (Finney ~~Cecil~~ et al., 2014; ~~Lopez 2016~~). A are often utilized to evaluate the performance of different lightning schemes. A
67 new lightning scheme proposed by Finney et al. (2014), which is based on upward cloud ice flux, has shown better spatial
68 and temporal correlation coefficients and root mean square errors (RMSEs) than the cloud top height scheme compared
69 against the LIS/OTD lightning observations. Another lightning scheme also showed more accurate lightning prediction than
70 the cloud top height scheme, which is also adopted in the ECMWF forecasting system (Lopez, 2016). This lightning scheme
71 uses Q_R (a quantity intended to represent the charging rate of collisions between graupel and other types of hydrometeors
72 inside the charge separation region), convective available potential energy (CAPE), and convective cloud-base height to
73 compute the lightning flash rate (Lopez, 2016). The two new lightning schemes ~~described~~(Finney et al., 2014; Lopez 2016)
74 mentioned above have only been ~~validated~~evaluated in a few chemical transport and climate models. The new lightning
75 schemes ~~must~~ are expected to be ~~validated~~evaluated and compared in more chemical transport and climate models, such as
76 CHASER. To achieve better prediction accuracy for lightning and better quantification of LNO_x in chemical climate models,
77 comparing and optimizing the existing lightning schemes and ~~validating~~evaluating them with various observation data are
78 also important.

79

80 Lightning simulations are also fundamentally important in chemical climate model studies for predictions of atmospheric
81 chemical fields and climate. Nevertheless, different lightning schemes respond very differently on decadal to multi-decadal
82 time scales under global warming. Some lightning schemes such as those using cloud top height or ~~convective available~~
83 ~~potential energy (CAPE)~~CAPE \times precipitation ~~rate~~ as a proxy for calculating lightning indicate that lightning increases
84 concomitantly with increasing global average temperature. By contrast, other lightning schemes, such as those using
85 convective mass flux or upward cloud ice flux as a proxy of lightning, indicate that lightning will decrease as the global
86 average temperature increases (Clark et al., 2017; Finney et al., 2018). Several studies (Price and Rind 1994; Zeng et al.,
87 2008; Jiang and Liao 2013; Banerjee et al., 2014; Krause et al., 2014; Clark et al., 2017) have found 5–16% increases in
88 lightning flashes per degree of increase in global mean surface temperatures with the lightning scheme based on cloud top
89 height. Over the ~~continental~~contiguous United States (CONUS), the CAPE \times precipitation ~~rate~~ proxy predicted a $12 \pm 5\%$
90 increase in the CONUS lightning flash rate per degree of global mean temperature increase (Romps et al., ~~2014~~-2014).
91 Compared to the findings reported by Romps et al. (2014), Finney et al. (2020) found a relatively small response of lightning
92 to climate change ($2\% \text{ K}^{-1}$) over Africa using a cloud-ice-based parametrisation for lightning. By contrast, Finney et al.
93 (2018) found a 15% global mean lightning flash rate decrease with the lightning scheme based on upward cloud ice flux in
94 2100 under a strong global warming scenario. Furthermore, a 2.0% decrease in global mean lightning flashes per degree of
95 increase in the global mean surface temperature with the lightning scheme based on convective mass flux has been reported
96 by Clark et al. (2017). Although it remains unclear which lightning scheme is best suited to predicting future lightning
97 (Romps, 2019), comparing different lightning schemes in different chemical climate models is valuable for consideration of
98 the sensitivity of lightning to global warming.

99
100 This study introduced ~~two~~three new lightning schemes into CHASER (MIROC). The first lightning scheme (Finney et al.,
101 2014) is based on upward cloud ice flux. The second one (Lopez, 2016), also adopted in the ECMWF forecasting system,
102 calculates lightning flash rates as a function of ~~the frozen precipitation convective flux, Q_R~~ (defined in Sect. 2.2), CAPE, and
103 convective cloud-base height. In the case of the second lightning scheme, by tuning the equations and adjustment factors
104 based on a study reported by McCaul et al. (2009), a new ~~modified version of the second~~ lightning scheme named ECMWF-
105 McCAUL scheme was also tested for CHASER (MIROC). ~~This~~The ECMWF-McCAUL scheme calculates lightning flash
106 rates as a function of CAPE and column precipitating ice. Our study conducted detailed ~~validation~~evaluation of lightning and
107 LNO_x by LIS/OTD lightning observations, NASA/ATom aircraft observations, and TROPOMI satellite observations. The
108 effects of different lightning schemes on the atmospheric chemical fields were evaluated. Also, 20-year (2001–2020) ~~long-~~
109 ~~term~~historical trend analyses of lightning densities and LNO_x emissions simulated by different lightning schemes were
110 conducted. Based on the results, the effects of LNO_x emissions during 2001–2020 on tropospheric NO_x and O₃ column
111 trends were estimated and discussed.

112
113 Research methods, including the model description and experiment setup, are described in ~~section~~Sect. 2. In ~~section~~Sect. 3.1,
114 ~~validation~~the evaluation of lightning schemes using LIS/OTD lightning observations is explained. In ~~section~~Sect. 3.2, LNO_x
115 emission simulation by different lightning schemes is ~~verified~~evaluated with aircraft and satellite measurements. Section 3.3
116 presents a discussion of the effects of different lightning schemes on the atmospheric chemical fields. ~~Long-term~~Historical
117 trends of lightning simulated by different lightning schemes are analyzed and discussed in ~~section~~Sect. 3.4. Section 3.5
118 discussed how LNO_x emissions (2001–2020) trends influence the tropospheric NO_x and O₃ column trends. Section 4 presents
119 the discussions and conclusions ~~obtained from~~of this study.

120 2 Method

121 2.1 Chemistry-climate model

122 The model used for this study is the CHASER (MIROC) global chemical transport and climate model (Sudo et al., 2002;
123 Sudo and Akimoto, 2007; Watanabe et al. 2011; Ha et al., 2021), which incorporates consideration of detailed chemical and
124 transport processes in the troposphere and stratosphere. CHASER calculates the distributions of 94 chemical species and
125 reflects the effects of 269 chemical reactions (58 photolytic, 190 kinetic, 21 heterogeneous). Its tropospheric chemistry
126 incorporates consideration of Non-Methane Hydrocarbons (NMHC) oxidation and the fundamental chemical cycle of O_x–
127 NO_x–HO_x–CH₄–CO. Its stratospheric chemistry simulates chlorine-containing and bromine-containing compounds,
128 chlorofluorocarbons (CFCs), hydrofluorocarbons (HFCs), carbonyl sulfide (OCS), and N₂O. Furthermore, it simulates the
129 formation of polar stratospheric clouds (PSCs) and heterogeneous reactions on their surfaces. CHASER is coupled to the
130 MIROC AGCM ver. 5.0 (Watanabe et al., 2011). Grid-scale large-scale condensation and cumulus convection (Arakawa–
131 Schubert scheme) are used to simulate cloud/precipitation processes. Aerosol chemistry is coupled with the SPRINTARS
132 aerosol model (Takemura et al., 2009), which is also based on MIROC.

133

134 For this study, horizontal resolution used is T42 (2.8° × 2.8°), with vertical resolution of 36 σ-p hybrid levels from the
135 surface to approximately 50 km. The AGCM meteorological fields (u, v, T) simulated by MIROC were nudged towards the
136 six-hourly NCEP FNL data (<https://rda.ucar.edu/datasets/ds083.2/>, last access: 6 December 2021). Anthropogenic precursor
137 emissions such as NO_x, CO, O₃, SO₂, and VOCs were obtained from the HTAP-II inventory for 2008
138 (https://edgar.jrc.ec.europa.eu/dataset_htap_v2, last access: 6 December 2021), with biomass burning emissions from
139 MACC-GFAS (Inness et al., 2013). The monthly soil NO_x emissions used in CHASER (MIROC) are constant for each year
140 and are derived from Yienger and Levy (1995).

141 2.2 Lightning NO_x emission scheme

142 The lightning flash rate in CHASER is originally parameterized by cloud-top height (Price and Rind, 1992, 1993), with a “C-
143 shaped” NO_x vertical profile adopted (Pickering et al., 1998). The equations used to calculate the lightning flash rate by
144 cloud-top height are

$$145 F_l = 3.44 \times 10^{-5} H^{4.9} \quad (1)$$

$$146 F_o = 6.2 \times 10^{-4} H^{1.73} \quad (2)$$

147 where F represents the total flash frequency (~~fl. min⁻¹~~; fl. min⁻¹), H stands for the cloud-top height (~~km~~), and subscripts l
148 and o respectively denote the land and ocean (Price and Rind, 1992).

149

150 For this study, ~~two~~three new lightning schemes are implemented into CHASER (MIROC). One is based on upward cloud ice
151 flux. It calculates the lightning flash rate by the following equations, as described by Finney et al. (2014).

$$152 f_l = 6.58 \times 10^{-7} \phi_{ice} \quad (3)$$

$$153 f_o = 9.08 \times 10^{-8} \phi_{ice} \quad (4)$$

154 Therein, f_l and f_o respectively represent the flash density (~~fl. m⁻² s⁻¹~~) offl. m⁻² s⁻¹ over land and ocean. Also, ϕ_{ice} is the
155 upward cloud ice flux at 440 hPa (~~kg_{ice} m_{cloud}⁻² s⁻² s⁻¹~~) as calculated using

$$156 \phi_{ice} = \frac{q \times \Phi_{mass}}{c}, \quad (5)$$

157 where q denotes the specific cloud ice water content at 440 hPa (~~kg_{ice} kg_{air}⁻¹~~), Φ_{mass} stands for the updraught mass flux at 440
158 hPa (~~kg_{air} m_{cell}⁻² s⁻¹~~), and c represents the fractional cloud cover at 440 hPa (~~m_{cloud}² m_{cell}⁻²~~). The 440 hPa pressure level is chosen
159 because it is a representative pressure level of fluxes in deep convective clouds (Finney et al., 2014). Moreover, Romps

160 (2019) has proposed an alternative approach to applying the ICEFLUX scheme by using the upward cloud ice flux at 260-K
 161 isotherms instead of at 440 hPa isobars. As suggested by Romps (2019), the isotherm-alternative is more appropriate for
 162 climate change simulations because the charge separation zone will follow the isotherms instead of the isobars with climate
 163 change. The 260-K isotherm is chosen because it is close to the 440 hPa isobar based on a present-day tropical sounding and
 164 it lies within the mixed-phase regions of clouds (Romps, 2019). To distinguish the two different approaches to applying the
 165 ICEFLUX scheme, the isobar approach is abbreviated as ICEFLUX P and the isotherm-alternative is abbreviated as
 166 ICEFLUX T.

167
 168 Another new lightning scheme, also adopted in the ECMWF forecasting system, calculates lightning flash rates as a function
 169 of the ~~frozen precipitation convective flux~~, $CAPEQ_R$ (defined in equation 8), $CAPE$, and convective cloud-base height
 170 (Lopez, 2016) as

$$171 \quad f_T = \alpha Q_R \sqrt{CAPE} \min(z_{base}, 1800)^2, \quad (6)$$

172 where f_T is the total lightning flash density (fl. $\text{km}^{-2}\text{m}^{-2}\text{day}^{-1}\text{s}^{-1}$), z_{base} is the convective cloud-base height in km , α (fl.
 173 $\text{kg}^{-1}\text{m}^{-3}$) is a constant obtained after calibration against the LIS/OTD climatology, which is set to $95.581.11 \times 10^{-15}$ in this
 174 study. As explained by Lopez (2016), the number 1800 used in equation (6) is a constraint to let the term z_{base} remains
 175 constant after it exceeds 1800 m. Note that the equation (6) is standardized on base SI units. $CAPE$ (m^2s^{-2}) is diagnosed
 176 from the following equation.

$$177 \quad CAPE = \int_{z_{LFC}}^{z_{w=0}} \max\left(g \frac{T_v^u - \bar{T}_v}{T_v}, 0\right) dz \quad (7)$$

178 In that equation, g is the constant of gravity. Also, T_v^u and \bar{T}_v respectively denote the virtual temperatures in the updraft and
 179 the environment. The integral in equation (7) starts at the level of free convection z_{LFC} and stops at the level at which
 180 negative buoyancy is found ($w = 0$). Quantity Q_R (kg m^{-2}) is intended to represent the charging rate of collisions between
 181 graupel and other types of hydrometeors inside the charge separation region. It is empirically calculated as

$$182 \quad Q_R = \int_{z_0}^{z_{-25}} q_{graup} (q_{cond} + q_{snow}) \bar{\rho} dz, \quad (8)$$

183 where z_0 and z_{-25} signify the heights (m) of the 0° and -25°C isotherms, and q_{cond} denotes the mass mixing ratio of cumulus
 184 cloud liquid water (kg kg^{-1}). The respective amounts of graupel (q_{graup} ; kg kg^{-1}) and snow (q_{snow} ; kg kg^{-1}) are computed from the following equations for each vertical level of the model.

$$186 \quad q_{graup} = \beta \frac{P_f}{\bar{\rho} V_{graup}} \quad (9)$$

$$187 \quad q_{snow} = (1 - \beta) \frac{P_f}{\bar{\rho} V_{snow}} \quad (10)$$

188 In those equations, P_f denotes the vertical profile of the frozen precipitation convective flux ($\text{kg m}^{-2}\text{s}^{-1}$), $\bar{\rho}$ stands
 189 for the environmental air density (kg m^{-3}), and V_{graup} and V_{snow} respectively express the typical fall speeds for
 190 graupel and snow set to 3.0 and 0.5 m s^{-1} . The dimensionless coefficient β is set as 0.7 for land and 0.45 for ocean to
 191 account for the observed lower graupel contents over oceans.

192
 193 For the original ECMWF scheme, by tuning the ~~convective cloud base height~~, the calculation equations, based on findings
 194 reported by McCaul et al. (2009), and the adjustment factors for land and ocean, the lightning prediction accuracy is
 195 improved further, as explained in Section 3.1. We named the new lightning scheme as ECMWF-
 196 McCAUL scheme, and it simulates the lightning flash rate by the following equations.

$$197 \quad f_l = \alpha_l Q_{Ra} CAPE^{1.3} \quad (11)$$

$$198 \quad f_o = \alpha_o Q_{Ra} CAPE^{1.3} \quad (12)$$

199 Therein, f_l and f_o respectively denote the total flash density of (fl. m⁻² s⁻¹) over land and ocean. Also, α_l and α_o are constants
 200 (fl. s^{1.6} kg⁻¹ m^{-2.6}) obtained after calibration against LIS/OTD climatology, respectively, for land and ocean. For this
 201 study, α_l and α_o are set respectively to $2.3667 \times 10^{-5} 10^{-16}$ and $1.4568 \times 10^{-6} 10^{-17}$. Then CAPE is computed in the
 202 same way as the original ECMWF scheme. In addition, Q_{Ra} (kg m⁻²) is a proxy for the charging rate resulting from the
 203 collisions between graupel and hydrometeors of other types inside the charge separation region (from 0° to -25°C isotherm),
 204 as reported by McCaul et al. (2009). Also, Q_{Ra} represents the total volumetric amount of precipitating ice in the charge
 205 separation region, calculated as

$$206 \quad Q_{Ra} = \int_{z_0}^{z_{-25}} (q_{graup} + q_{snow} + q_{ice}) \bar{\rho} dz, \quad (13)$$

207 where z_0 and z_{-25} respectively stand for the heights of the 0° and -25°C isotherms, and q_{graup} , q_{snow} , and q_{ice} respectively
 208 represent the mass mixing ratios (kg kg⁻¹) of graupel, snow, and cloud ice. In this study, q_{graup} and q_{snow} were computed
 209 respectively by equations (9) and (10). For the modified ECMWF-McCAUL scheme, V_{graup} and V_{snow} are set respectively to
 210 3.1 and 0.5 m s⁻¹. Then q_{ice} was diagnosed using Arakawa–Schubert cumulus parameterization.

211

212

Table 1: Basic information of all lightning schemes assessed for this study

Abbreviation	Parameter	Remark
CTH (Price, C., & Rind, D., 1994)	Cloud top height	Originally used in CHASER (MIROC)
ICEFLUX (Finney et al., 2014)	Upward cloud ice flux at 440 hPa isobar (ICEFLUX_P) or at 260-K isotherm (ICEFLUX_T)	The 440 hPa level is used as a pressure level representative of fluxes in deep convective clouds
ECMWF-original (Lopez, 2016)	<ul style="list-style-type: none"> • Q_R (Described in equation 8) • CAPE • Convective cloud-base height 	Also adopted in the ECMWF forecasting system
ECMWF-McCAUL	<ul style="list-style-type: none"> • Column precipitating ice • CAPE 	Equations and adjustment factors are modified from the original ECMWF scheme. Equations are modified based on findings reported by McCaul (McCaul et al., 2009)

213

214 Table 1 presents all the lightning schemes examined for this study. As described in this paper, the original ECMWF scheme
 215 and the modified ECMWF-McCAUL scheme are designated collectively as ECMWF schemes. The NO emission per flash
 216 used in CHASER for all lightning schemes was set to 111 moles NO per recent studies, the intra-
 217 cloud (IC) lightning flash and 1113 moles NO per flashes are as efficient as the cloud-to-ground (CG) lightning flash as
 218 parameters, as explained by Price (1997), the lightning NO_x production efficiency (LNO_x PE) is
 219 reported to be 100–400 mol per flash (Ridley et al., 1997; Cooray et al., 2009; Ott et al., 2010; Allen et al., 2019).
 220 Therefore, the LNO_x PE values of IC and CG used in CHASER are set to the same value (250 mol per flash), which is the
 221 median of the commonly cited range of 100–400 mol per flash.

222

223 A fourth-order polynomial is used to calculate the proportion of total flashes that are cloud-to-ground (p) based on the cloud
 224 depth, as described in an earlier report (Price and Rind, 1993).

$$225 \quad p = \frac{1}{64.09 - 36.54D + 7.493D^2 - 0.648D^3 + 0.021D^4}. \quad (14)$$

226 In that equation, D represents the depth of cloud above the 0°C isotherms in kilometres.

227

228 A “C-shaped” vertical profile for LNO_x emission is used initially in CHASER (MIROC). However, a recent report of work
 229 by Ott et al. (2010) indicated that a “C-shaped” vertical profile of LNO_x might place too much mass near the surface and too
 230 little in the middle troposphere. A new LNO_x vertical profile named the “backward C-shaped” profile was subsequently
 231 proposed by Ott et al. (2010). It was tested in this study using CHASER (MIROC).

232 **2.3 Observation data for model evaluation**

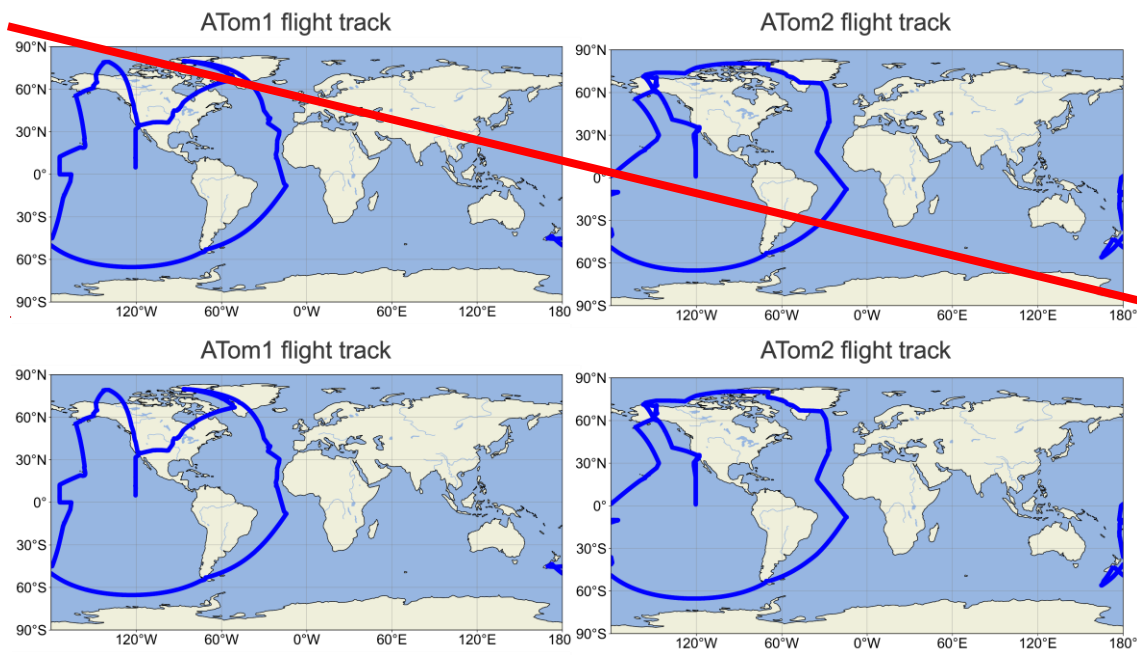
233 **2.3.1 Lightning observations**

234 The LIS/OTD gridded climatology datasets are used for this study, consisting of climatologies of total lightning flash rates
235 observed using the Lightning Imaging Sensor (LIS) and spaceborne Optical Transient Detector (OTD): OTD aboard the
236 MicroLab-1 satellite and LIS aboard the Tropical Rainfall Measuring Mission (TRMM) satellite (Cecil et al., 2014). Both
237 sensors detect lightning by monitoring pulses of illumination produced by lightning in the 777.4 nm atomic oxygen multiplet
238 above background levels. Both sensors, in low ~~earth~~Earth orbit, view an ~~earth~~Earth location for about 3 min as OTD passes
239 overhead or for 1.5 min as LIS passes overhead. Actually, OTD and LIS circle the globe 14 times a day and 16 times a day,
240 respectively. OTD collected data between +75 and -75° latitude from May 1995 through March 2000, whereas LIS observed
241 between +38 and -38° latitude from January 1998 through April 2015.

242

243 The product used throughout this paper is the LIS/OTD 2.5 Degree Low Resolution Time Series (LRTS). The LRTS
244 includes the daily lightning flash rate on a 2.5° regular latitude–longitude grid from May 1995 through April 2015.

245



246

247

Figure 1: ATom1 and ATom2 flight tracks.

248 **2.3.2 Atmospheric tomography (ATom) aircraft observations**

249 To ~~validate~~evaluate the LNO_x emissions calculated by different lightning schemes, we used NO observation by the
250 atmospheric tomography (ATom) aircraft missions (Wofsy et al., 2018). By deploying an extensive gas and aerosol payload
251 on the NASA DC-8 aircraft, ATom is designed to sample the atmosphere systematically on a global scale, performing
252 continuous profiling from 0.2 to 12 km altitude. Flights took place in each of the four seasons of 2016 through 2018. ~~To~~
253 ~~validate~~Since most of the LNO_x emissions in different seasons lightning occurs over land regions during summer, ATom1
254 (July–August 2016) and ATom2 (January–February 2017) were used ~~for validation to evaluate LNO_x emissions~~
255 (corresponding to summer in the northern and southern hemispheres, respectively). Both ATom1 and ATom2 originate from
256 the Armstrong Flight Research Center in Palmdale, California, USA, fly north to the western Arctic, south to the South
257 Pacific, east to the Atlantic, north to Greenland, and return to California across central North America. Figure 1 exhibits the
258 respective flight tracks of ATom1 and ATom2. To evaluate the model simulated NO against the ATom observations, we
259 have sampled the specific flight track and timings from the modelled data.

260 2.3.3 TROPOMI satellite observations

261 Tropospheric Monitoring Instrument (TROPOMI) is the payload on-board the Sentinel-5 Precursor (S5P) satellite of the
262 European Space Agency (ESA), which was launched in October 2017. TROPOMI has been providing observations of
263 important atmospheric pollutants (NO_2 , O_3 , CO , CH_4 , SO_2 , CH_2O) with an unprecedented horizontal resolution of approx. 7
264 $\times 3.5 \text{ km}^2$ since August 2017 (changed to $5.5 \times 3.5 \text{ km}^2$ after August 2019). ~~For this study, the TROPOMI observations in~~
265 ~~2019 for the NO_2 tropospheric column were used to validate the LNO_x emissions simulated by different lightning~~
266 ~~schemes~~The data used in this study is the TROPOMI level-2 offline (OFFL) tropospheric NO_2 columns in 2019. The product
267 version is 1.0.0 from 2019-01-01 to 2019-03-20 and updated to 1.1.0 from 2019-03-21 to 2019-12-31. For the direct
268 comparisons between TROPOMI level-2 products with CHASER results, the following procedures were conducted to pre-
269 process the TROPOMI data and CHASER modelled fields.

270 1. The TROPOMI retrievals with quality assurance (QA) values of ≥ 0.75 were selected.

271 2. Horizontally, the TROPOMI data (tropospheric NO_2 columns, temperatures, pressures, averaging kernels) were
272 interpolated to the CHASER $2.8^\circ \times 2.8^\circ$ grid.

273 3. The modelled results were sampled based on the TROPOMI overpass time. The CHASER tropospheric NO_2 columns
274 were calculated by using the sampled modelled results, the averaging kernels retrieved from the TROPOMI retrievals, and
275 the temperature and pressure profiles provided by TROPOMI retrievals. The averaging kernels are applied to each layer of
276 the CHASER outputs following the equation (16).

277 4. The pre-processed data described above were used to produce the monthly averaged data.

278 2.3.4 OMI satellite observations

279 Ozone Monitoring Instrument (OMI) is a key instrument onboard NASA's Aura satellite for measuring criteria pollutants
280 such as O_3 , NO_2 , SO_2 , and aerosols. OMI has been providing observations with spatial resolution varying from $13 \text{ km} \times 25$
281 km to $26 \text{ km} \times 128 \text{ km}$ since October 2004 (Goldberg et al., 2019). The NO_2 product used in this study is the level-3 daily
282 global gridded ($0.25^\circ \times 0.25^\circ$) Nitrogen Dioxide product (OMNO2d) (Nickolay et al. 2019). The O_3 product used in this
283 study is the monthly mean tropospheric column O_3 product developed from OMI in combination with Aura Microwave
284 Limb Sounder (MLS) with the detailed method described by Ziemke et al. (2006).

285 2.4 Experiment setup

286 For this study, all the introduced lightning schemes were implemented into CHASER (MIROC). Six sets of experiments
287 were conducted for this study, ~~as~~ and the detailed settings of all experiments are presented in Table 2. For each set of
288 experiments, the same initial conditions and chemical emissions were used except for LNO_x emissions. The set of
289 experiments that applied meteorological nudging also has the same meteorological conditions. The monthly varying soil NO_x
290 emissions used are constant each year for all experiments derived from Yienger and Levy (1995). All experiments used the
291 “backward C-shaped” LNO_x vertical profile (Ott et al., 2010). The LNO_x PE values of IC and CG used in all experiments are
292 set to the same value (250 mol per flash), which is based on the recent literature (Ridley et al., 2005; Cooray et al., 2009; Ott
293 et al., 2010; Allen et al., 2019). It is noteworthy that there still exist large uncertainties in determining the LNO_x PE values
294 (Allen et al., 2019; Bucselo et al., 2019) and the choice of different LNO_x PE values may influence the simulated LNO_x
295 emissions and chemical fields. A more sophisticated parametrisation of LNO_x PE values needs to be implemented and
296 verified in the chemistry-climate models in future research.

298 The first set of experiments was conducted for the years of 2001–2020. It was used to ~~validate~~evaluate the distribution of the
299 lightning flash rate against LIS/OTD lightning observations and to derive the ~~long-term~~historical lightning trend. The second
300 set of experiments is the same as the first set of experiments, but ~~using~~uses daily mean LNO_x emission rates of 2001

301 calculated using lightning schemes for each year. This set of experiments is used to produce results for comparison with
 302 those of the first set of experiments to estimate the effects of LNO_x emission trends on tropospheric NO_x and O₃ column
 303 trends. The third set of experiments gives results for 2011–2020. These experiments are used to estimate the effects of
 304 different lightning schemes on atmospheric chemical fields. To normalize the different annual LNO_x emission amounts by
 305 different lightning schemes, temporally and spatially uniform adjustment factors were applied to adjust the mean LNO_x
 306 production (2011–2020) of all lightning schemes to 5.0 TgN yr⁻¹. Note the 10-years (2011–2020) mean LNO_x production was
 307 adjusted to 5.0 TgN yr⁻¹ but the LNO_x production in each year is not exactly 5.0 TgN yr⁻¹. This adjustment was achieved by
 308 first conducting the simulations without any adjustment and the 2011–2020 mean LNO_x production (P_{LNO_x}) was calculated,
 309 then the corresponding adjustment factor (adj_factor) can be calculated by using ~~different adjustment factors: the following~~
 310 equation.

$$311 \quad adj_factor = \frac{5.0}{P_{LNO_x}} \quad (15)$$

312 Similarly, we also adjusted the LNO_x emissions in the fourth to the sixth sets of experiments to 5.0 TgN yr⁻¹. The fourth set
 313 of experiments is for 2016, with the fifth set ~~is~~ for 2017. These two sets of experiments were conducted to compare model
 314 results with ATom1 and ATom2 aircraft observations. The sixth set of experiments is for 2019. It is conducted to
 315 ~~validate~~ evaluate model results using TROPOMI satellite observations.

316 **Table 2: All experiments in this study**

Number	1st		2nd		3rd	4th	5th	6th
Period	2001–2020	2001–2020	2001–2020	2001–2020	2011–2020	2016	2017	2019
Nudging	On	Off ^a	On	Off	On	On	On	On
LNO _x emissions	Interactively calculated ^b	Interactively calculated	Fixed to 2001	Fixed to 2001	Interactively calculated	Interactively calculated	Interactively calculated	Interactively calculated
Adjusted to 5.0 TgN yr ⁻¹	No	No	No	No	Yes	Yes	Yes	Yes
Climate ^c	2001-2020 (RCP4.5)	2001-2020 (RCP4.5)	2001-2020 (RCP4.5)	2001-2020 (RCP4.5)	2011-2020 (RCP4.5)	2016 (RCP4.5)	2017 (RCP4.5)	2019 (RCP4.5)
Anthropogenic emissions	HTAP-II (2008) for all years							
Soil NO _x emissions	Monthly varying values but constant for each year derived from Yienger and Levy (1995)							
Biomass burning emissions	MACC (2001-2020)	MACC (2001-2020)	MACC (2001-2020)	MACC (2001-2020)	MACC (2011-2020)	MACC (2016)	MACC (2017)	MACC (2019)

317
 318 ~~All experiments used the “backward C-shaped” LNO_x vertical profile. The NO emissions per flash were set to 111 moles NO~~
 319 ~~per IC (intro cloud lightning flash) and 1113 moles NO per CG (cloud to ground lightning flash) as parameters drawn from~~
 320 ~~work reported by Price et al. (1997).~~

321 ^aNudging off means the meteorological fields (u, v, T) are free-running instead of nudging towards the NCEP FNL data.

322 ^bLNO_x is interactively calculated by using different lightning schemes.

323 ^cThe climate change is simulated by prescribed SST/sea ice fields and prescribed varying concentrations of GHGs (CO₂,
 324 N₂O, methane, chlorofluorocarbons – CFCs – and hydrochlorofluorocarbons – HCFCs) utilized only in the radiation scheme.
 325 The SST/sea ice fields are obtained from the HadISST dataset (Rayner et al., 2003).

326 3 Results and Discussion

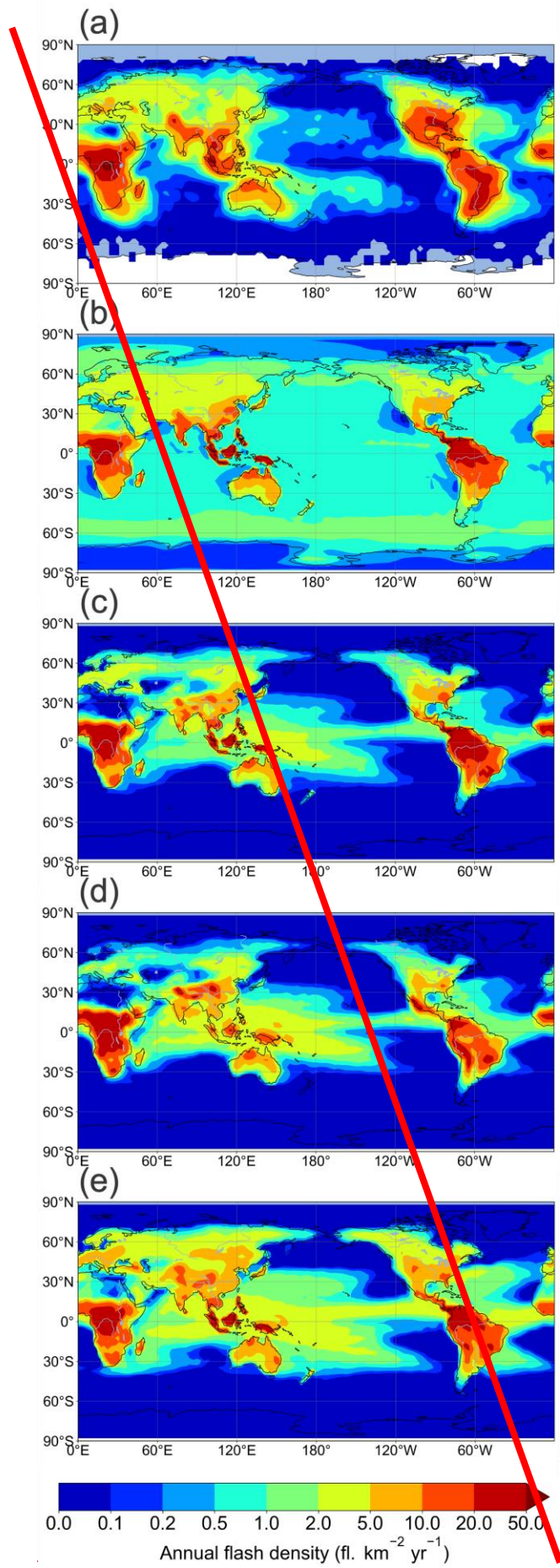
327 3.1 ~~Validation~~ Evaluation of the lightning schemes

328 ~~To validate model results with lightning observation data in a broader range (between +75° and -75° latitude), lightning~~
 329 ~~prediction accuracy for all introduced lightning schemes was compared with the climatological lightning distributions of~~
 330 ~~OTD (1996–2000). Figure 2 presents a global map of the OTD annual mean lightning density spanning 1996–2000 and~~
 331 ~~mean lightning density during 2007–2011, as simulated using different lightning schemes. Figure 3 displays a Taylor~~

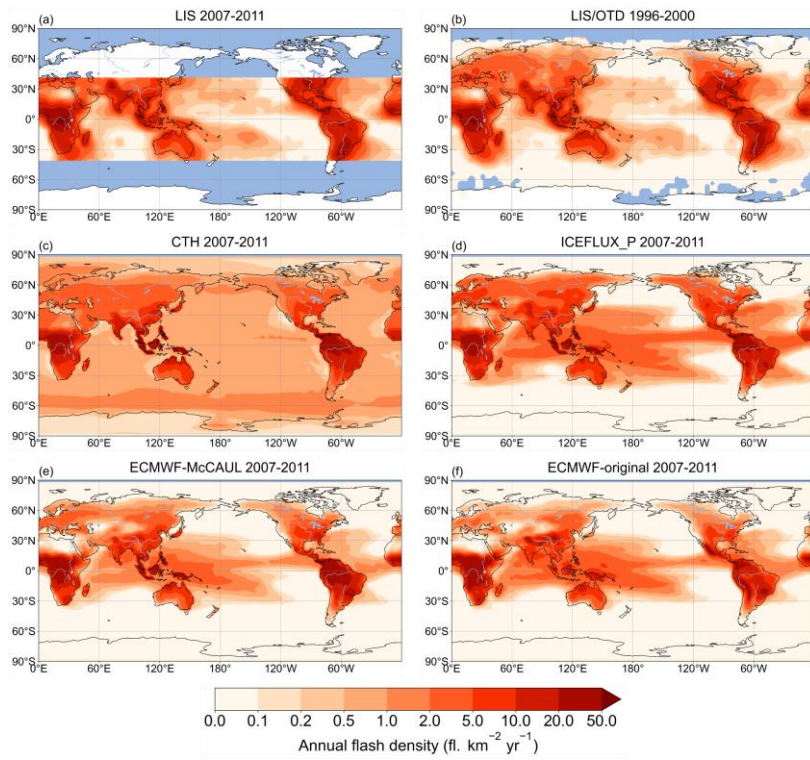
332 diagram, which presents the prediction accuracy of various lightning schemes in 2007–2011 simulations compared to the
333 OTD 1996–2000 lightning climatology. As investigated by Finney et al. (2014), 5 years data are necessary and appropriate to
334 produce a lightning climatology. Therefore, model results with nudging (2007-2011) were evaluated against the
335 climatological lightning distributions of LIS (2007-2011) within $\pm 38^\circ$ latitude and LIS/OTD (1996-2000) within a broader
336 range of $\pm 75^\circ$ latitude. We have evaluated the potential uncertainties associated with the inconsistency of the time period of
337 simulated lightning and observed lightning (2007-2011 and 1996-2000). The statistical analysis between LIS (2007-2011)
338 and LIS/OTD (1996-2000) within $\pm 38^\circ$ latitude exhibits an extremely high spatial correlation coefficient ($R=0.99$) and
339 relatively small relative bias (0.65%), which supports the reasonability of comparing model results with the observation data
340 within different time range.

341
342 The distribution of lightning observed by LIS/OTD and simulated by CHASER (MIROC) with different lightning schemes is
343 depicted in Fig. 2. Figure 2 shows that lightning over the ocean is not well reproduced by the original CTH scheme.

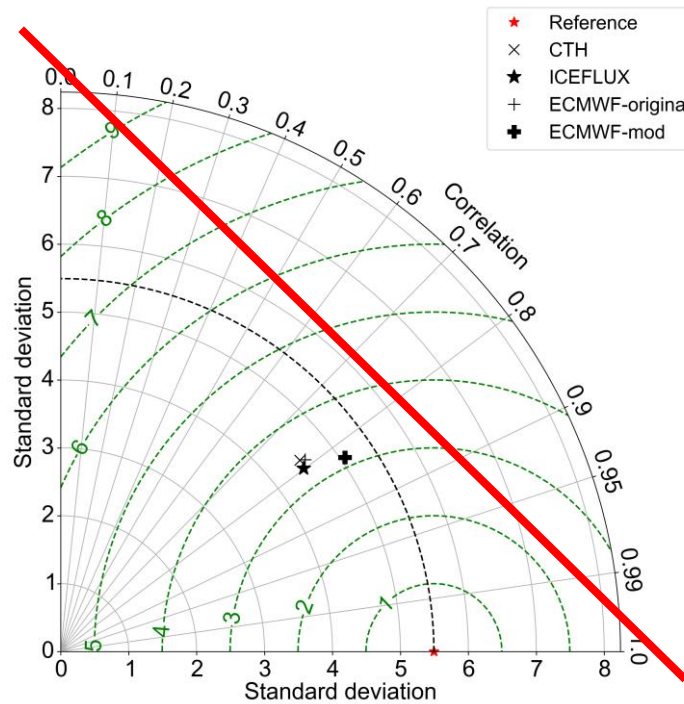
344 Actually, it is improved considerably by the new lightning schemes. Compared with the CTH scheme, the original ECMWF
345 scheme better represents the lightning distribution in South Asia including the Indian region. The ECMWF schemes and the
346 ICEFLUX_P scheme reduced negative biases in North America compared to the CTH scheme. In Australia, the ECMWF
347 schemes better simulate the horizontal distribution of lightning. All lightning schemes failed to capture the worldwide
348 maximum value found over the Congo Basin, although all lightning schemes captured the active region in central Africa.



349
350

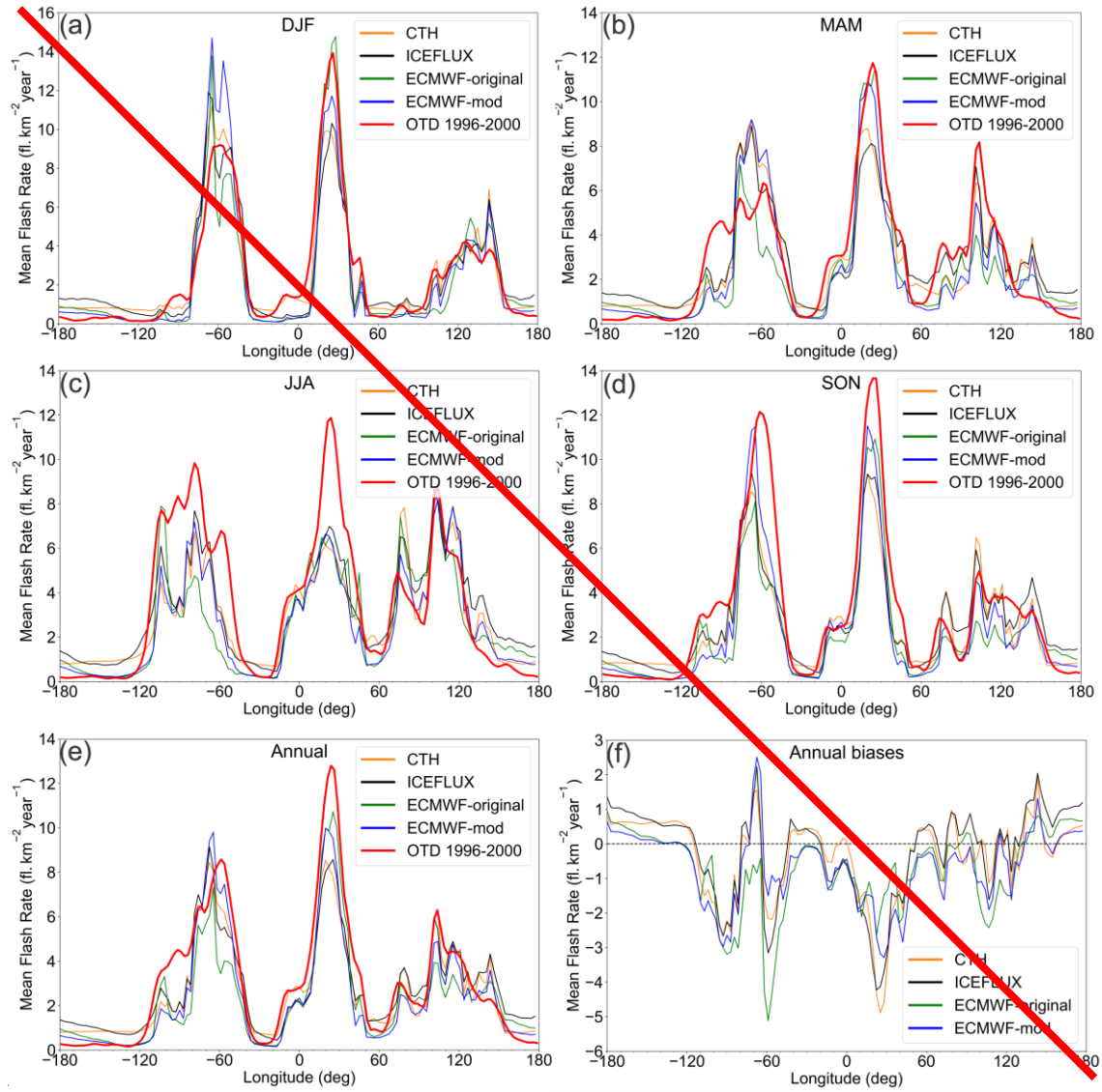


351
 352 **Figure 2: Annual mean lightning flash densities from (a) LIS satellite observations spanning 2007–2011, (b) LIS/OTD satellite**
 353 **observations spanning 1996–2000, (c) the CTH scheme in 2007–2011, (d) the ICEFLUX_P scheme in 2007–2011, (e) the**
 354 **ECMWF-McCAUL scheme in 2007–2011, and (f) the original ECMWF**
 355 **scheme in 2007–2011.**

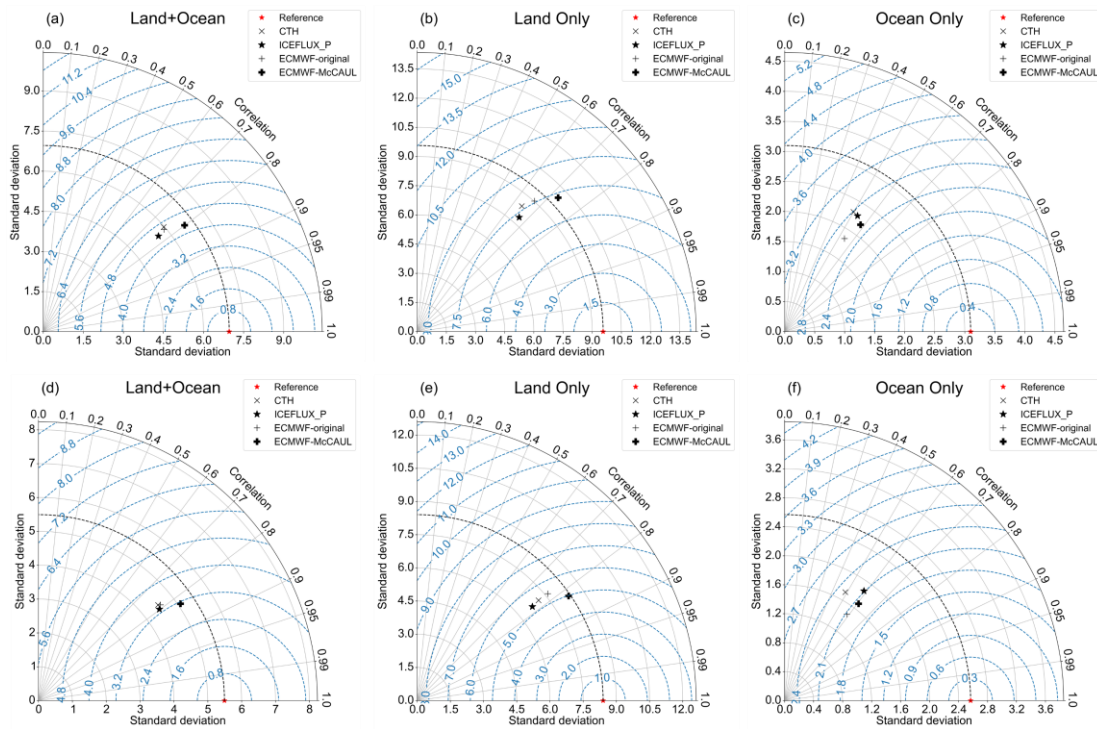


356
 357 **Figure 3: Taylor diagram showing**
 358 **To directly estimate the prediction accuracy of various lightning schemes, the Taylor diagrams are displayed in 2007–2011**
 359 **simulations compared to the OTD 1996–2000.** In Fig. 3a, the overall prediction accuracy of the ICEFLUX_P and original
 360 **ECMWF schemes evaluated against the LIS 2007–2011 lightning climatology:**
 361
 362 **In Fig. 3 is slightly improved compared to the CTH scheme. This improvement is more obvious when considering land and**
 363 **ocean separately (Figs. 3b-c). In the case of Figs. 3a-c, the ECMWF-McCAUL scheme has shown the best prediction**
 364 **accuracy among all lightning schemes. In Fig. 3d, comparison of the annual mean lightning flash rate of LIS/OTD 1996–**
 365 **2000 and the CHASER calculation for 2007–2011 yields spatial correlation coefficients of 0.80 and 0.79 for the**
 366 **ICEFLUX_P and original ECMWF schemes, respectively, which are slightly higher than that found for the CTH**
 367 **(0.78). The overall RMSE of the ICEFLUX_P scheme is 3.34 fl. km⁻² yr⁻¹, which is slightly less than that of the CTH**

368 scheme of $3.44 \text{ fl. km}^{-2} \text{ yr}^{-1}$. Among all lightning schemes, the modified-ECMWF-McCAUL scheme exhibits the highest
 369 spatial correlation coefficient (0.83) and the lowest RMSE ($3.20 \text{ fl. km}^{-2} \text{ yr}^{-1}$)- $\text{km}^{-2} \text{ yr}^{-1}$) as depicted in Fig. 3d. As displayed
 370 in Fig. 2, the prediction accuracy of lightning over the ocean is significantly improved, which can also be verified in Fig. 3f.



371

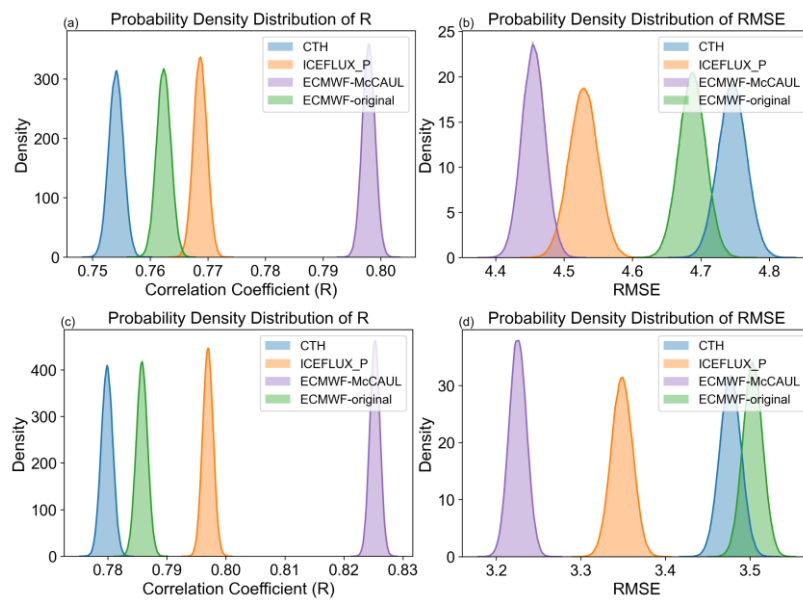


372
373
374
375

Figure 3: Taylor diagram showing the prediction accuracy of various lightning schemes in 2007–2011 simulations compared to the LIS 2007–2011 lightning climatology (a-c) and the LIS/OTD 1996–2000 lightning climatology (d-f).

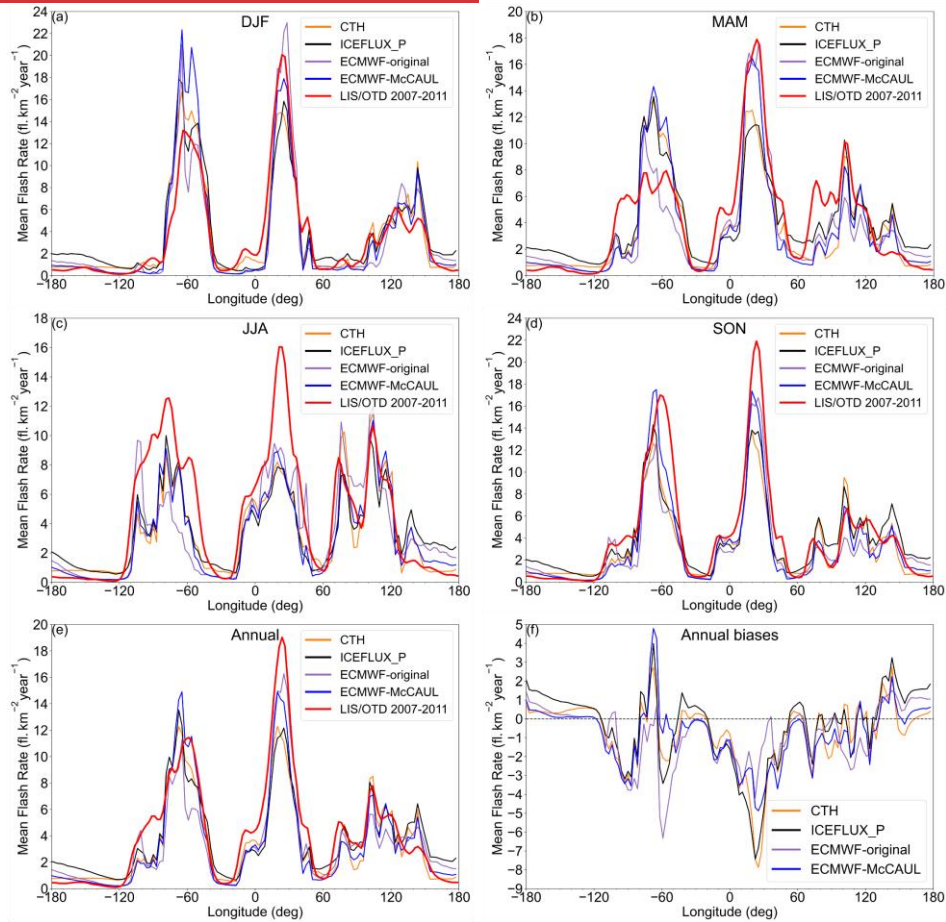
376
377
378
379
380
381
382
383
384
385
386
387

To estimate whether the improvement of prediction accuracy discussed in Fig. 3 is significant, a significant test is conducted by considering the uncertainties in the LIS/OTD observations. Based on the uncertainties in the LIS/OTD observations, the probability density distributions (PDDs) of spatial correlation coefficients (R) and RMSE between the model and observations are derived by using a Monte Carlo method and displayed in Fig. 4. The uncertainties in the LIS/OTD observations are determined based on the uncertainties of the instrument bulk flash detection efficiency of LIS ($88 \pm 9\%$) and OTD ($54 \pm 8\%$) (Boccippio et al., 2002). The R and RMSE shown in Fig. 4 are all normally distributed which is determined by the Kolmogorov–Smirnov test. Based on the probability density functions of R and RMSE derived from Fig. 4, the order of R between the model and observations is estimated to be $\text{ECMWF-McCAUL} > \text{ICEFLUX_P} > \text{ECMWF-original} > \text{CTH}$ with a confidence limit larger than 99.9%. Moreover, the order of RMSE between the model and observations is estimated to be $\text{ECMWF-McCAUL} < \text{ICEFLUX_P} < \text{ECMWF-original}$ and CTH with a confidence limit larger than 95%. According to the significant test described above, we can conclude that the newly implemented lightning schemes have improved the lightning prediction accuracy compared to the original CTH scheme.



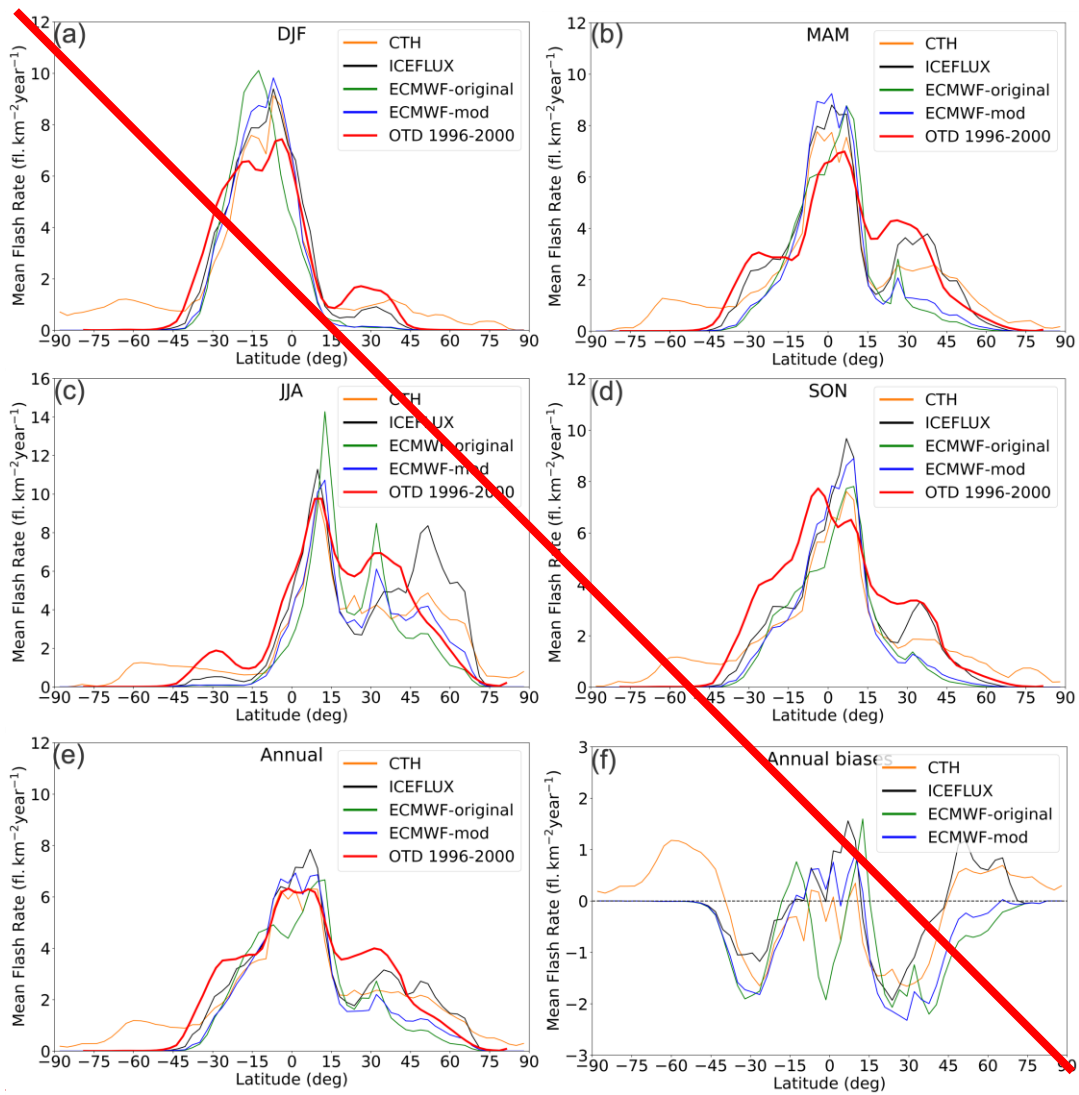
388

389 **Figure 4: The probability density distributions (PDDs) of spatial correlation coefficients (R) and RMSE between the model and**
 390 **LIS/OTD lightning observations. Figures 4(a–b) show the PDDs obtained between LIS lightning climatology (2007–2011) and the**
 391 **model outputs (2007–2011) within $\pm 38^\circ$ latitude. Figures 4(c–d) show the PDDs obtained between LIS/OTD lightning climatology**
 392 **(1996–2000) and the model results (2007–2011) within $\pm 75^\circ$ latitude.**

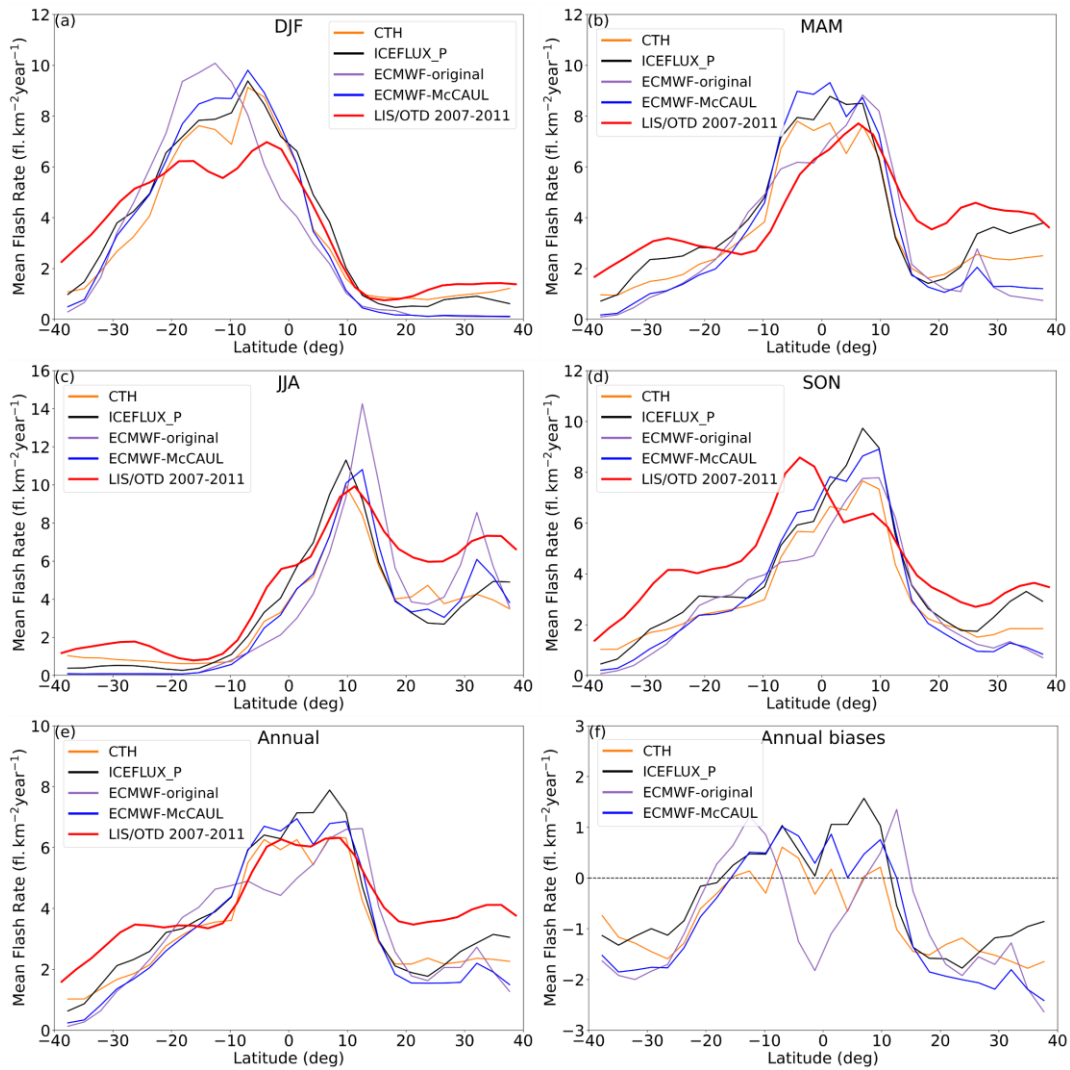


393 **Figure 5: Seasonal and annual meridional average lightning flash densities distribution from OTD 1996–2000–LIS 2007–2011**
 394 **climatology (red line) and from simulation results (2007–2011) obtained using different lightning schemes. The meridional average**
 395 **is only taken within the OTDLIS viewing region of $\pm 75/38^\circ$ latitude. The biases (model-obs.) in Fig. 4e5e are also portrayed in Fig.**
 396 **4f5f.**
 397
 398

399 Figure 45 displays a comparison of seasonal and annual meridional average lightning flash densities from simulations
 400 (2007–2011) and OTDLIS satellite observations (1996–2000/2007–2011). As Fig. 45 shows, the pairs of curves are usually
 401 in good agreement, even though the annual plot (Fig. 5e) highlights the underestimation which occurs for Africa (from 0
 402 degrees to 30 degrees east) and North America (from 80 degrees west to 120 degrees west). The ECMWF schemes have
 403 made improvements within Africa. Also, the ICEFLUX_P scheme has P and the original ECMWF schemes have slightly
 404 reduced the biases over North America. A noticeable underestimation over the Americas in JJA and overestimation in MAM
 405 can be observed respectively in Figs. 4e5c and 4b5b. Lightning densities over Africa are generally underestimated to varying
 406 degrees in different seasons, with the greatest underestimation occurring in JJA (Fig. 4e5c). Lightning densities over Asia
 407 (from 60 degrees east to 120 degrees east) are slightly underestimated in MAM (Fig. 4b5b). The ICEFLUX_P scheme has
 408 reduced the biases.



409
 410 **Figure 5: Seasonal and annual zonal average lightning flash densities distribution from OTD 1996–2000 climatology (red line) and**
 411 **from the simulation results obtained using different lightning schemes. The**
 412 **Figure 6 is the same as Fig. 5 biases (model-obs.) in Fig. 5f are also presented in Fig. 5f.**
 413
 414 **Figure 5 is the same as Fig. 4, but for the zonal mean distributions. The curves of the model results and the observation**
 415 **results in Fig. 5f generally show good agreement. Figure 5f shows that, overall, the ICEFLUX scheme P and modified the**
 416 **ECMWF scheme-McCAUL schemes slightly overestimated the lightning densities near the equator (5°W–510°S–10°N).**
 417 **All lightning schemes underestimated the lightning densities within 15°N–4538°N and 15°S–4520°S–38°S. Figure 5f also**
 418 **shows that the ICEFLUX P scheme has reduced the biases within 1510°N–4538°N and 15°S–4538°S. Furthermore, Fig. 5f**
 419 **shows that both the ICEFLUX scheme and compared to the CTH scheme overestimated the flash densities within 45°N–**
 420 **90°N. Only the CTH scheme overestimated the flash densities within 45°S–90°S. In DJF (Fig. 5a6a), all lightning schemes**
 421 **overestimated the flash densities over the low latitude region regions but slightly underestimated the flash densities over the**
 422 **middle latitude regions in the Southern Hemisphere. In MAM (Fig. 5b6b), lightning densities are overestimated near the**
 423 **equator and underestimated over 15°N–4538°N and 15°S–4538°S by all lightning schemes to varying degrees. In JJA (Fig.**
 424 **5e6c), noticeable overestimation around 10°N by the original ECMWF scheme is apparent. Moreover, the CTH and the**
 425 **original ECMWF schemes respectively facilitated reduction of model biases over 15°S–4538°S and 15°N–4538°N. Figure**
 426 **5e also exhibits that the ICEFLUX scheme vastly overestimated the flash densities over 45°N–75°N. As Fig. 5d6d shows,**
 427 **the model-predicted lightning maximum value is shifted approximately 15 degrees to the north in SON compared to the**
 428 **lightning observations. Figure 5d6d also shows that all lightning schemes underestimated the lightning densities over 15°N–**
 429 **4538°N and 0°–38°S. The ICEFLUX P scheme has shown improvement over this region these regions.**



430
 431 **Figure 6: Seasonal and annual zonal average lightning flash densities distribution from LIS 2007–2011 climatology (red line) and**
 432 **from the simulation results (2007–2011) obtained using different lightning schemes. The biases (model-obs.) in Fig. 6e are also**
 433 **presented in Fig. 6f.**

434 **3.2 Validation/Evaluation of LNO_x emissions**

435 **3.2.1 Validation/Evaluation of LNO_x emissions by ATom1 and ATom2 observations**

436 To verify/evaluate the LNO_x emissions of different lightning schemes, we used ATom1 and ATom2 aircraft measurements
 437 (NO) for comparison against model results. All lightning schemes, when implemented in CHASER, produce flash rates
 438 corresponding to global annual LNO_x emissions within the range estimated by Schumann and Huntrieser (2007) of 2–8 TgN
 439 yr⁻¹. To eliminate differences in annual total LNO_x emissions by different lightning schemes, we chose to adjust the annual
 440 LNO_x emissions of all lightning schemes to 5.0 TgN yr⁻¹ by applying adjustment factors. The “backward C-shaped” LNO_x
 441 vertical profile is applied to all lightning schemes.

442

443

444

445

446

447

448

449

450

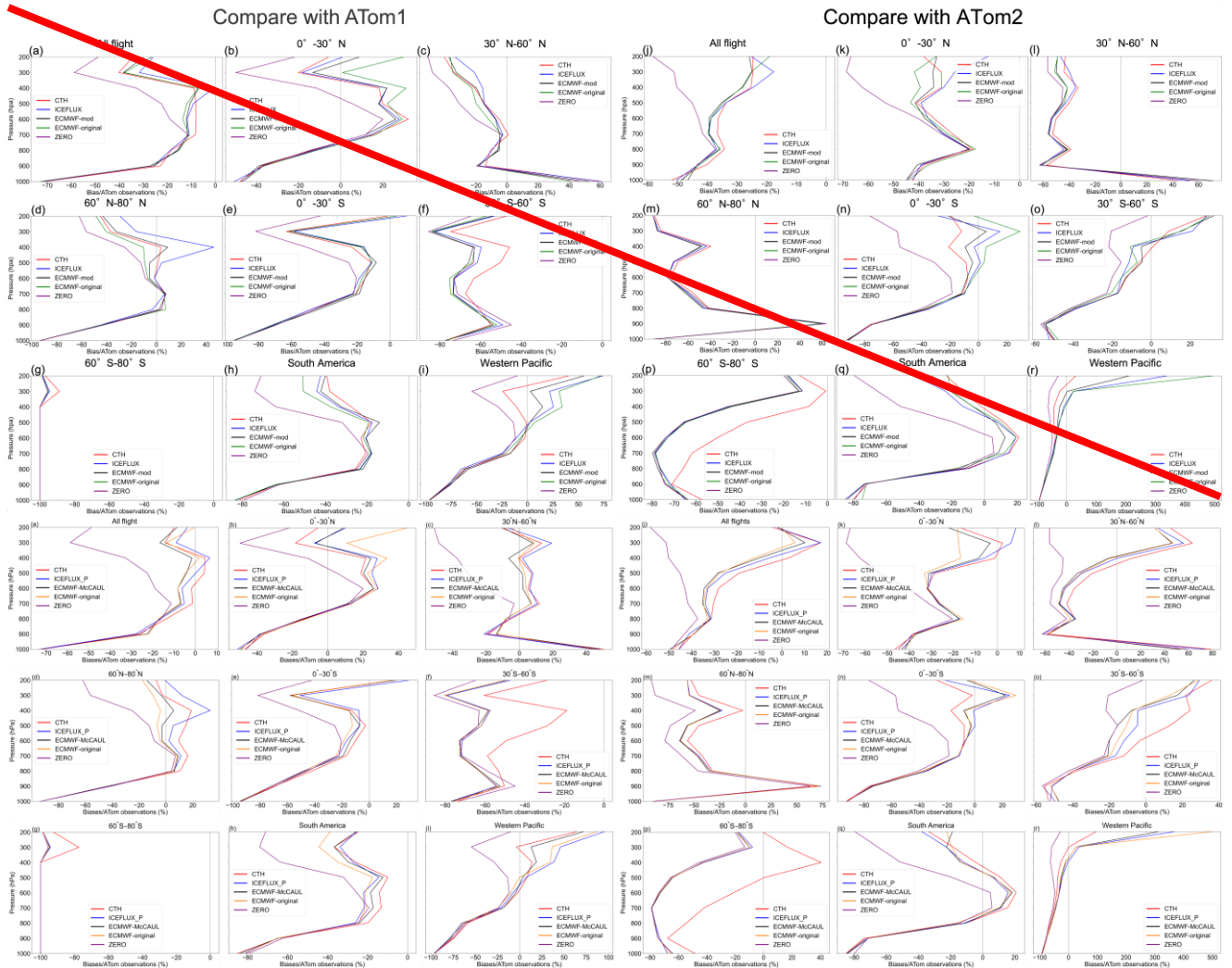


Figure 67: Vertical profile of biases/ATom1 observations (a–i) and the vertical profile of biases/ATom2 observations (j–r). The bias is the model bias (NO) against ATom observations. Data for each pressure level P are calculated within the range of $P \pm 50$ hPa. South America is the region of 0° – 30° S, 0° – 30° W. The Western Pacific is the region of 10° N– 30° S, 160° E– 160° W.

Table 3: Model biases (NO) when compared against ATom1 (upper panel) and ATom2 (lower panel). The unit is ppt. The biases within the South America region (0 – 30° S, 0 – 30° W) and Western Pacific region (10° N– 30° S, 160° E– 160° W) are also shown in this table.

Lightning scheme	All flight	0° – 30° N	30° N– 60° N	60° N– 80° N	0° – 30° S	30° S– 60° S	60° S– 80° S	South America	Western Pacific
CTH	-6.54	-3.22	-0.50	-13.06	-9.33	-12.32	-7.55	-6.79	-3.03
ICEFLUX_P	-5.18	0.31	1.15	-9.16	-8.21	-16.21	-8.28	-7.00	0.08
ECMWF-McCAUL	-6.99	0.13	-1.05	-14.80	-9.43	-16.42	-8.29	-7.17	-2.24
ECMWF-original	-5.48	7.03	0.28	-16.66	-9.59	-16.38	-8.30	-8.71	-0.72
ZERO	-19.00	-11.02	-20.85	-32.98	-15.91	-17.35	-8.34	-13.77	-8.63
Lightning scheme	All flight	0° – 30° N	30° N– 60° N	60° N– 80° N	0° – 30° S	30° S– 60° S	60° S– 80° S	South America	Western Pacific
CTH	-0.91	-2.57	5.80	-6.18	-11.11	3.61	1.45	-19.16	-4.70
ICEFLUX_P	-1.04	-0.76	3.98	-6.81	-7.45	2.82	-4.88	-22.02	3.01
ECMWF-McCAUL	-1.73	-3.71	2.81	-6.89	-3.71	1.81	-5.33	-12.24	1.20
ECMWF-original	-1.95	-5.26	2.96	-6.87	-2.74	1.58	-5.23	-13.90	3.55
ZERO	-12.66	-15.51	-11.08	-9.77	-28.40	-4.18	-5.94	-47.68	-13.14

451

452

453

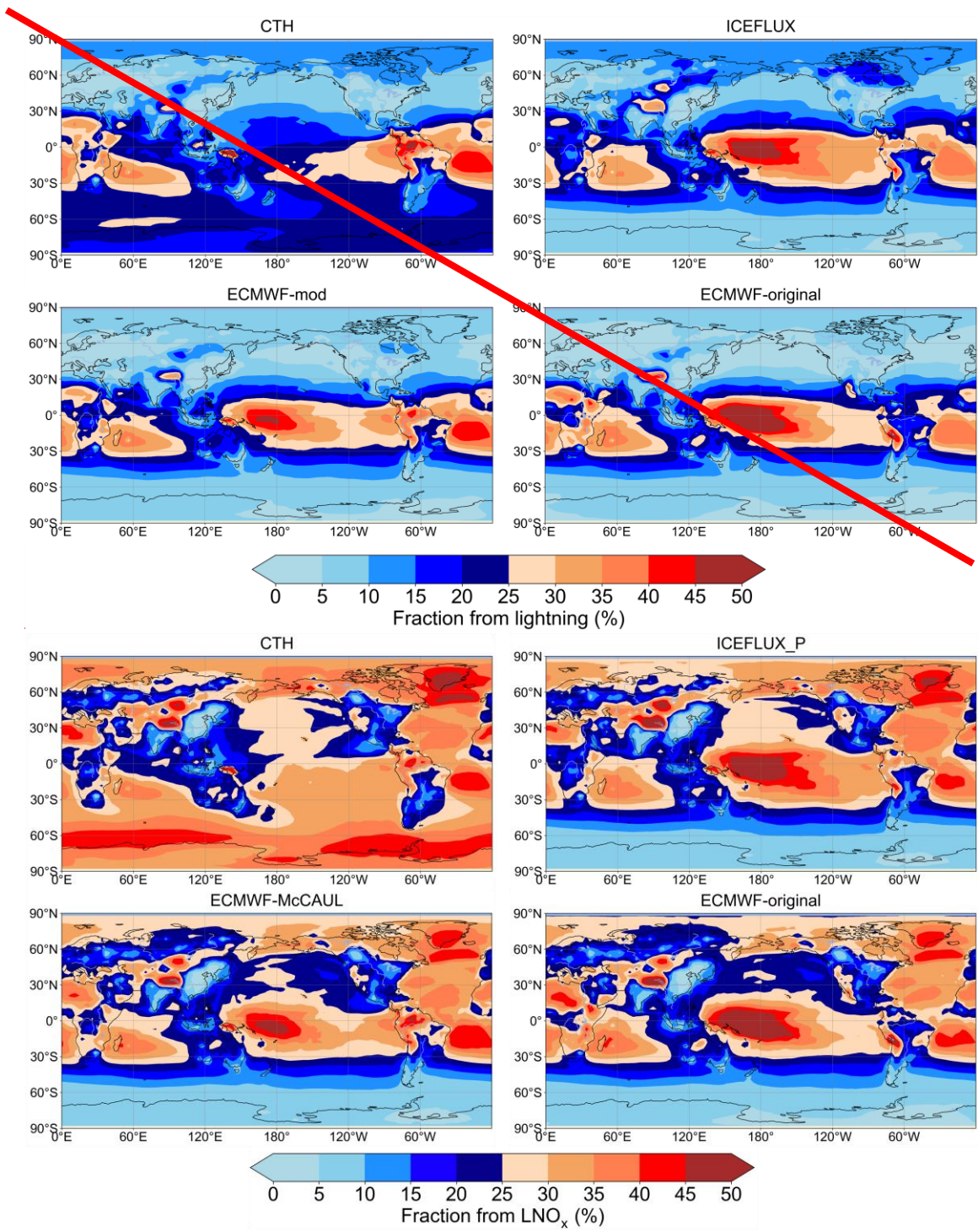
454

455

Table 3 presents model biases of different lightning schemes against the ATom1 and ATom2 observations. Figure 67 displays the vertical profile of biases/ATom observations in percentage terms. In Table 3 and Fig. 67, case ZERO is the case with the lightning flash, with LNO_x emissions completely switched off. Comparisons between model results and ATom observations were conducted within two specific regions (South America region and Western Pacific region) in which LNO_x

456 is the major source of NO_x (Fig. 7). ~~From comparison of the results simulated using the CTH scheme with the “C-shaped” or~~
457 ~~the “backward C-shaped” LNO_x vertical profile against ATom measurements, we found that the total model biases were~~
458 ~~slightly reduced by application of the “backward C-shaped” LNO_x vertical profile compared to the “C-shaped” LNO_x~~
459 ~~vertical profile. As Table 3 and Fig. 68). As Table 3 and Fig. 7 show, the model generally tends to underestimate the NO~~
460 concentrations. The model biases are reduced considerably by including lightning NO_x sources. For ATom1, overall, the
461 ICEFLUX_P scheme has the smallest model bias. The ~~original ECMWF schemes~~ scheme also reduced the model biases
462 compared to the CTH scheme (Table 3). ~~The ICEFLUX P and the ECMWF-McCAUL schemes reduced the model biases~~
463 ~~substantially within 0°–30°N latitude where the lightning activities are most dominant during the ATom1 observation period~~
464 ~~(2016-07-29 ~ 2016-08-23). In the range of 30°S to 80°N in ATom1, overall the ICEFLUX_P scheme reduced the model~~
465 ~~biases considerably. Also, and the ECMWF schemes slightly reduced or extended the model biases compared to the CTH~~
466 ~~scheme (Table 3, Figs. 6a7b–e). However, in the range of 30°S–80°S, the model biases were slightly extended by the~~
467 ~~ICEFLUX_P and the ECMWF schemes compared to the CTH scheme (Table 3, Figs. 6f7f–g). This finding is consistent with~~
468 ~~Fig. 5c, in which the lightning densities predicted by the CTH scheme are larger than other lightning schemes in the~~
469 ~~Southern Hemisphere in JJA.~~

470
471 For ATom2, overall, the ~~ICEFLUX scheme and the original ECMWF schemes~~ schemes slightly reduced the model biases over
472 the upper troposphere, compared to the CTH scheme (Fig. 6j). ~~The 7j). During the ATom2 observation period (2017-01-26 ~~~
473 ~~2017-02-21), the lightning activities are most dominant within the range of 0°–30°S, where the model biases were reduced~~
474 ~~significantly by newly implemented lightning schemes. A hotspot of lightning activities during the ATom2 observation~~
475 ~~period is the South America region, where the model biases were reduced dramatically by the ICEFLUX scheme~~
476 ~~over ECMWF schemes. The model biases were mostly reduced by the newly implemented lightning schemes within the low~~
477 ~~latitude region but were extended over the and middle-latitude to regions, but slightly extended within the high-latitude~~
478 ~~region compared to the CTH scheme (Figs. 6k–p). regions. The model biases were mostly reduced or extended over the~~
479 middle to upper troposphere (Fig. 67). This is true because most LNO_x was distributed over the middle to upper troposphere.
480 Also, NO_x has a longer lifetime over the middle to upper troposphere. In the Western Pacific region, results obtained from
481 comparisons with ATom1 and ATom2 indicate that ~~the CTH scheme underestimated, and the other all lightning~~ schemes
482 overestimated LNO_x emissions in the upper troposphere; also, both the ICEFLUX_P scheme and ECMWF schemes reduced
483 the total model biases considerably more than the CTH scheme did.



484

485

486 **Figure 78:** Sensitivity of simulated tropospheric NO₂ columns to LNO_x emissions using different lightning schemes in 2019. NO₂
 487 column because of LNO_x emissions was determined as the difference between the simulation with LNO_x emissions and a simulation
 488 that excludes LNO_x emissions.

489

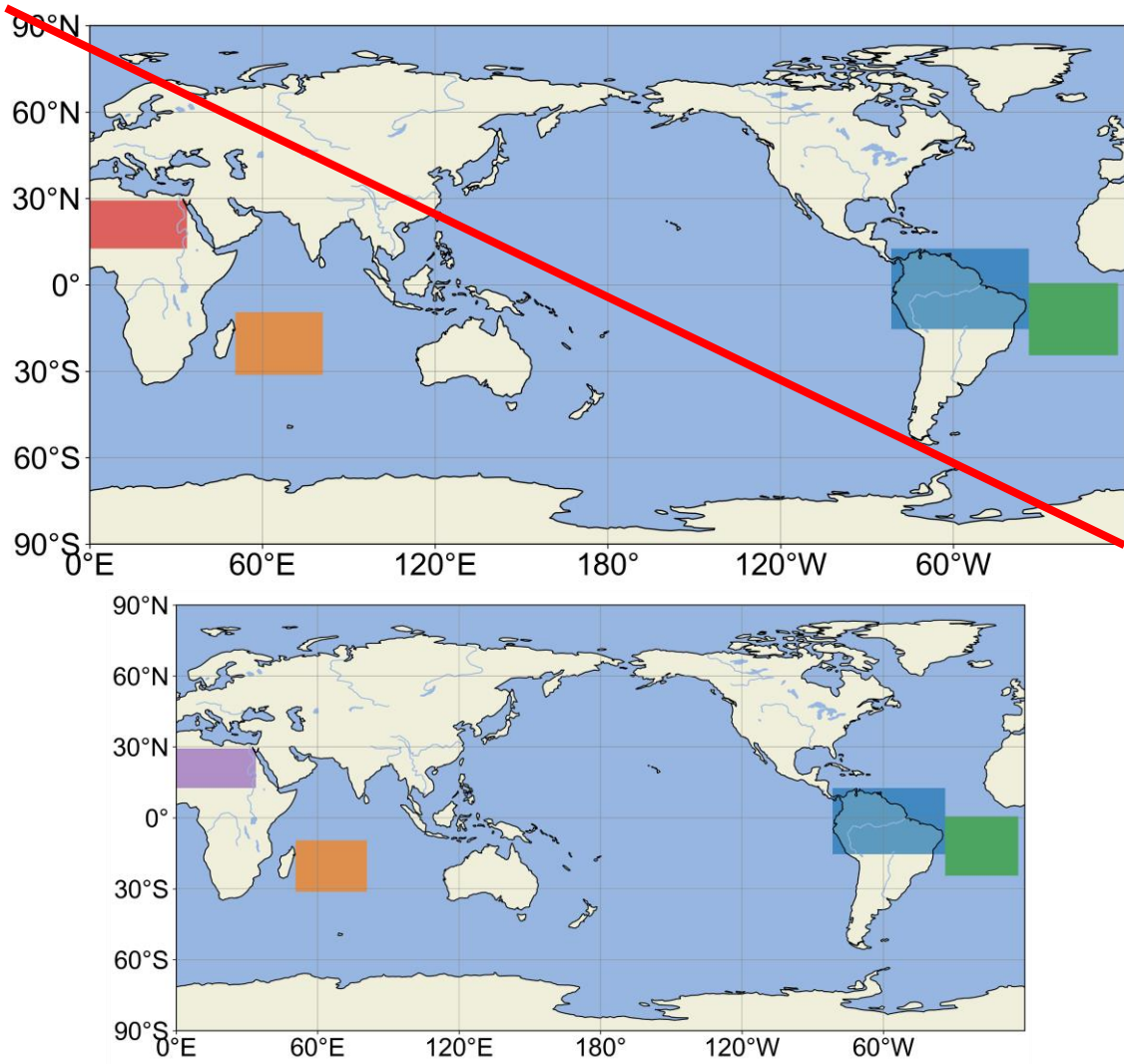
490 **3.2.2 Validation/Evaluation of LNO_x emissions by TROPOMI satellite observations**

491 TROPOMI satellite observations of NO₂-tropospheric NO₂ columns were used to ~~verify~~ evaluate LNO_x emission results
 492 obtained using the CHASER model. To eliminate differences in annual total LNO_x emissions attributable to the different
 493 lightning schemes, we adjusted the annual LNO_x emissions of all lightning schemes to 5.0 TgN yr⁻¹ using different
 494 adjustment factors. For direct comparison between CHASER and TROPOMI NO₂-tropospheric NO₂ columns, the averaging
 495 kernel information from TROPOMI observations was used. The averaging kernels were applied to CHASER outputs
 496 following Eq. (4516).

497
$$X_{chaser} = \sum_{i=1}^N A_{tropomi} x_{chaser} \tag{4516}$$

498 In that equation, X_{chaser} represents the CHASER NO_2 -tropospheric NO_2 column after averaging kernels applied, $A_{tropomi}$
499 denotes the TROPOMI averaging kernels, x_{chaser} denotes the CHASER NO_2 partial column at layer i , and N denotes the
500 number of tropospheric layers.

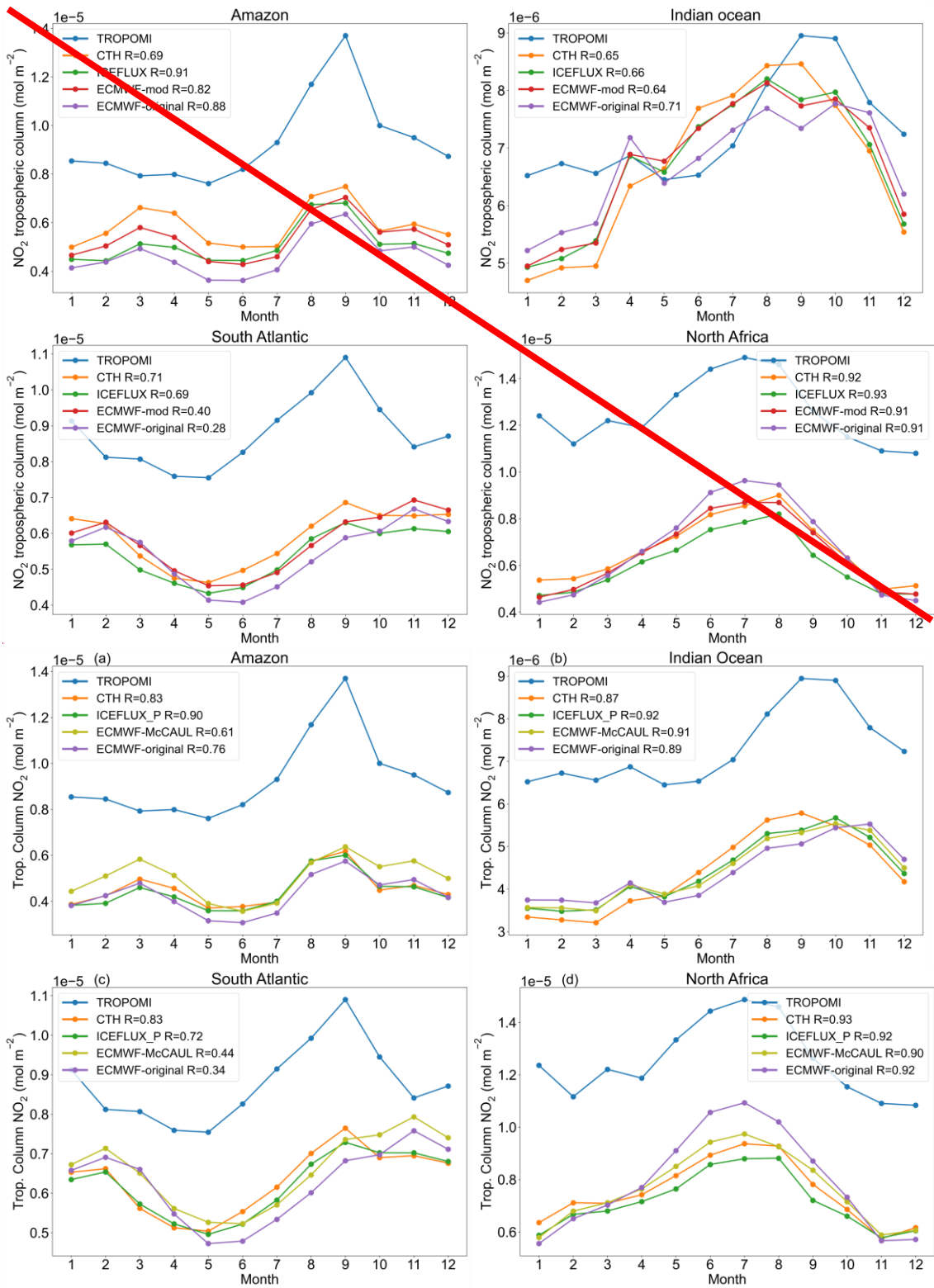
501



502

503 **Figure 89:** Four target regions for which LNO_x is the major source of NO_x . The four target regions are North Africa (~~red~~purple),
504 Indian Ocean (~~yellow~~orange), Amazon (blue), and South Atlantic (green).

505



506

507

508 **Figure 910:** Comparisons of smoothed CHASER and TROPOMI (blue) NO_2 -tropospheric NO_2 columns over four target regions in
 509 2019. Legends show the temporal correlation coefficients.

510

511 Comparison between TROPOMI observations and CHASER outputs indicates that the CHASER model tends to
 512 underestimate NO_2 -tropospheric NO_2 columns. Overall, the ICEFLUX scheme has shown the smallest model bias newly
 513 implemented lightning schemes have not shown improvements of NO_2 -model biases of tropospheric NO_2 columns- at an
 514 annual global scale. To validate the results minimize the uncertainties of model biases of tropospheric NO_2 columns caused
 515 by other factors, we chose to further and to compare evaluate the LNO_x emissions of different lightning schemes by
 516 TROPOMI observations, over four regions are chosen as target specific regions (Fig. 89), where LNO_x is the major source of
 517 NO_x- (as shown in Fig. 8).

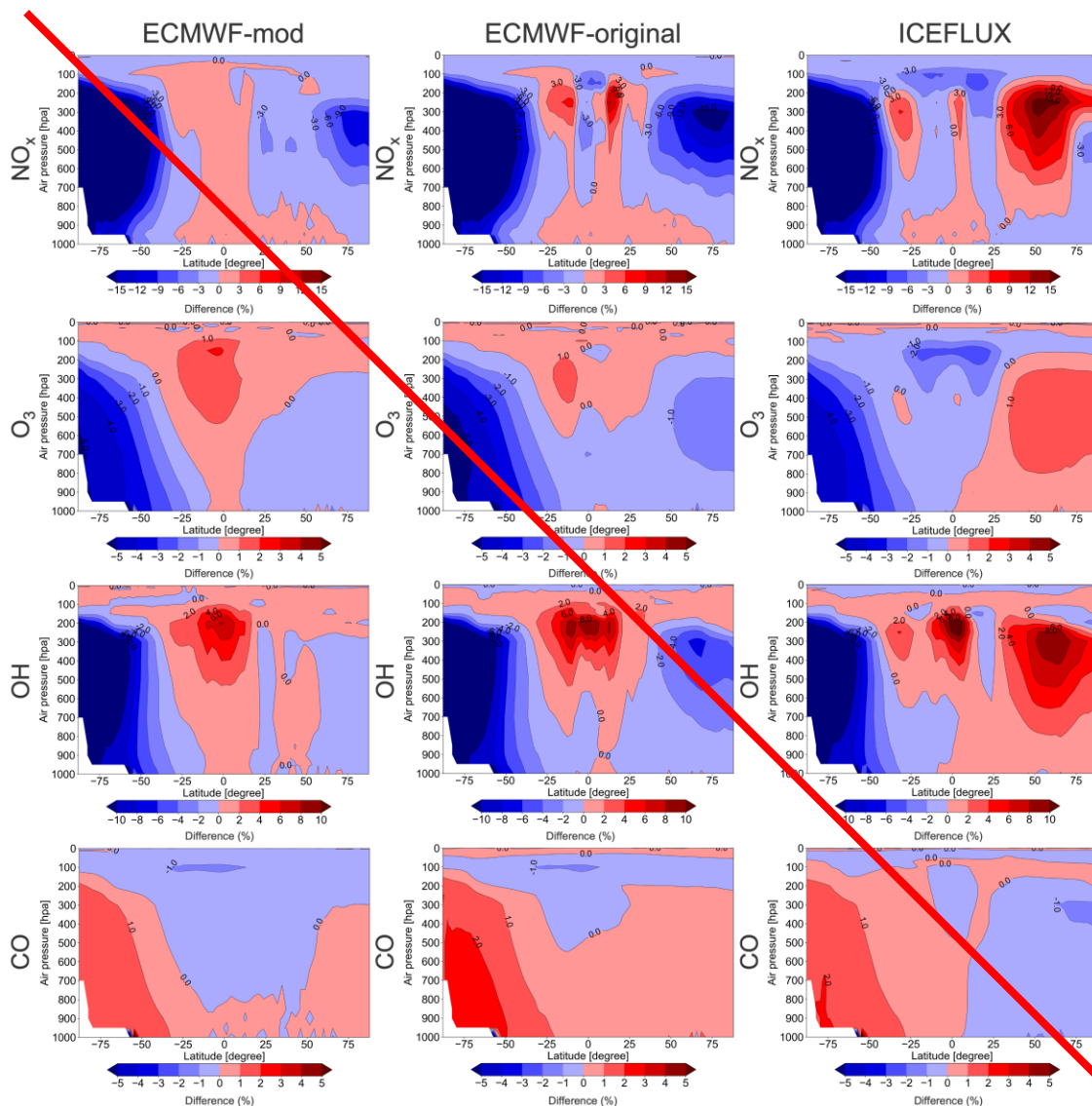
518 Figure 7 shows the sensitivity of tropospheric NO₂ columns to LNO_x emissions as simulated using different lightning
519 schemes. As Fig. 7 shows, the four regions presented in Fig. 8 are hotspots for LNO_x emissions. Therefore, these four
520 regions are chosen as the target regions. Figure 9-10 presents a comparison of smoothed CHASER and TROPOMI NO₂
521 tropospheric NO₂ columns over four target regions in 2019. The spatial average values of each month in 2019 are shown in
522 Fig. 9-10. That figure shows, generally, the model captured the temporal variation of NO₂ tropospheric columns, especially in
523 the land region (Amazon and North Africa). The ICEFLUX scheme showed good temporal correlation in all four regions,
524 with improved temporal correlation coefficients for three of them (Amazon, Indian Ocean, North Africa) tropospheric NO₂
525 columns in the four regions. Actually, the temporal variations of modelled tropospheric NO₂ columns are close to each other.
526 For the Amazon region, lightning activities are most dominant during MAM and SON, when the ECMWF-McCAUL
527 scheme has shown noticeable improvements in model biases (Fig. 10a). Figure 10b reveals that all the newly implemented
528 schemes slightly reduced the model biases with the original ECMWF scheme showing the smallest model biases during the
529 most prevailing season of lightning (DJF). Figure 10c is for the South Atlantic region where the most prevailing season of
530 lightning is also DJF. Figure 10c shows that the ECMWF schemes slightly reduced the model biases compared to the CTH
531 scheme. The ECMWF schemes have similar temporal correlation coefficients Referring to the CTH Fig. 10d, the dominant
532 season of lightning is JJA, when the ECMWF-original scheme in two target regions (Indian Ocean, North Africa). Compared
533 with the CTH scheme, the ECMWF schemes improved the temporal correlation coefficients in the Amazon region
534 considerably. However, the ECMWF schemes reduced the temporal correlation coefficients in the South Atlantic region,
535 mainly because of inconsistency between the model and the observed trends during April–June. reduced the model biases
536 and the ECMWF-McCAUL scheme also slightly reduced the model biases.

537 3.3 Effects of different lightning schemes on tropospheric chemical fields

538 In the tropospheric chemical field, LNO_x has an important role. The LNO_x effects on the tropospheric chemical fields vary
539 along with differences in the horizontal distribution of LNO_x in different lightning schemes. To evaluate the influences of
540 different lightning schemes on the tropospheric chemical fields, several ten-year (2011–2020) experiments were conducted
541 with the ten-year mean LNO_x production of all lightning schemes adjusted to 5.0 TgN yr⁻¹ (Section Sect. 2.4). CTH scheme
542 with a “backward C-shaped” profile is regarded as the base scheme. The effects of different lightning schemes on the
543 atmospheric chemistry are calculated as shown in Eq. (4617).

$$544 \text{Impact}_{ij} = \frac{(LS_{ij} - \text{Base}_j)}{\text{Base}_j} \quad (4617)$$

545
546 Therein, Impact_{ij} represents the effects of the i -th lightning scheme on the concentrations of target atmospheric component
547 j . Also, LS_{ij} denotes the concentrations of target atmospheric component j simulated by the i -th lightning scheme. Base_j
548 stands for the concentrations of target atmospheric component j as simulated using the base scheme.

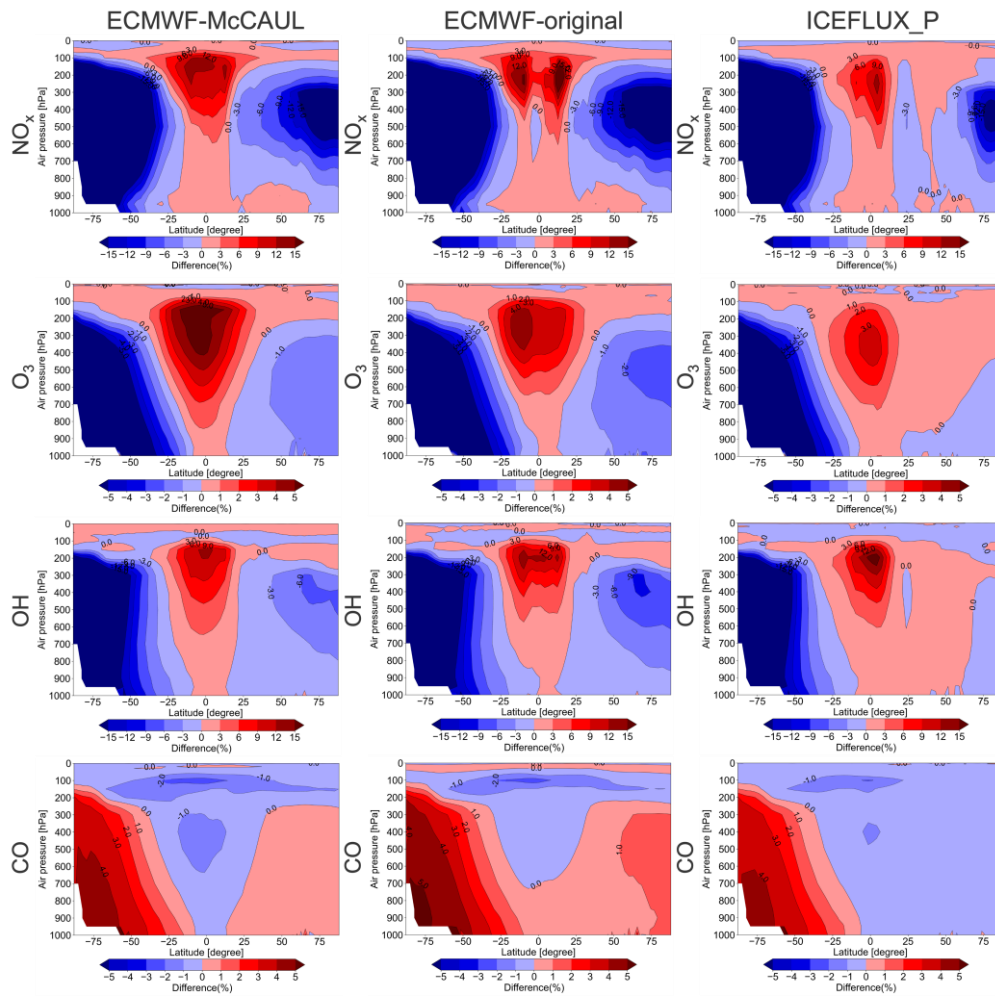


549

550 **Figure 10: Effects of modified ECMWF scheme, original ECMWF scheme, and ICEFLUX scheme on the atmospheric chemical**
 551 **fields (NO_x, O₃, OH, CO) on the zonal mean (%).**

552 **Figure 1011** presents the respective effects of the **modified-ECMWF-McCAUL**, original ECMWF, and ICEFLUX_P
 554 schemes on the atmospheric chemical fields (NO_x, O₃, OH, CO) relative to the base scheme CTH. The **modified-ECMWF-**
 555 **McCAUL** scheme led to an increase (~~approx.~~ **approximate maximum is 12%**) in NO_x concentration at low latitude regions
 556 and a decrease (~~approx.~~ **approximate maximum is 15%**) at middle to high latitude regions. In the case of the **modified**
 557 **ECMWF-McCAUL** scheme, the concentration of ozone and OH radical mostly increased at low latitude regions and
 558 decreased at middle to high latitude regions in the Southern Hemisphere, which corresponds to the changing pattern of NO_x.
 559 ~~Compared to the modified ECMWF scheme, The effects of~~ the original ECMWF scheme ~~caused a decrease rather than an~~
 560 ~~increase in ozone and OH radical concentrations in~~ the atmospheric chemical fields are similar to that of the ~~lower~~
 561 ~~troposphere at low latitude regions. Unlike the modified ECMWF-McCAUL scheme, overall. However,~~ the original
 562 ECMWF scheme led to ~~an increase in a~~ higher total tropospheric CO₂ burden compared to the ECMWF-McCAUL scheme.
 563 As Fig. ~~1011~~ shows, the three lightning schemes led to a marked decrease in NO_x, O₃, and OH radical concentrations over
 564 the South Pole region. This decrease occurred because the lightning densities and the LNO_x emissions simulated by the CTH
 565 scheme are markedly higher than those simulated using other lightning schemes at this latitude band (Fig. 2 ~~and Fig. 5e~~).
 566 Moreover, NO_x can engender the formation of ozone and OH radical. In the case of the ICEFLUX_P scheme, the
 567 concentrations of NO_x, ozone, and OH radical mostly increased in the ~~Northern Hemisphere tropics~~ and decreased ~~at middle~~
 568 ~~to high latitude regions~~ in the Southern Hemisphere.

570 Methane lifetime is an indicator reflecting the tropospheric oxidation capacity. The global mean tropospheric lifetime of
 571 methane against tropospheric OH radical spanning 2011–2020 with the CTH, original ECMWF, ~~modified-ECMWF-~~
 572 McCAUL, and ICEFLUX_P schemes are estimated respectively as 9.623226 years, 9.647299 years, 9.612256 years, and
 573 9.606229 years. Compared to the CTH scheme, the ~~original-ECMWF schemes~~ led to a slight increase in methane's
 574 global mean tropospheric lifetime. In contrast, the ~~modified-ECMWF and ICEFLUX schemes led to a slight decrease in~~
 575 methane's global mean tropospheric lifetime simulated by the ICEFLUX_P scheme is almost the same as that simulated by
 576 the CTH scheme. Although little difference exists in the total tropospheric oxidation capacity simulated by different
 577 lightning schemes, the ECMWF schemes and ICEFLUX_P scheme led to marked changes of oxidation capacity in different
 578 regions of the troposphere.



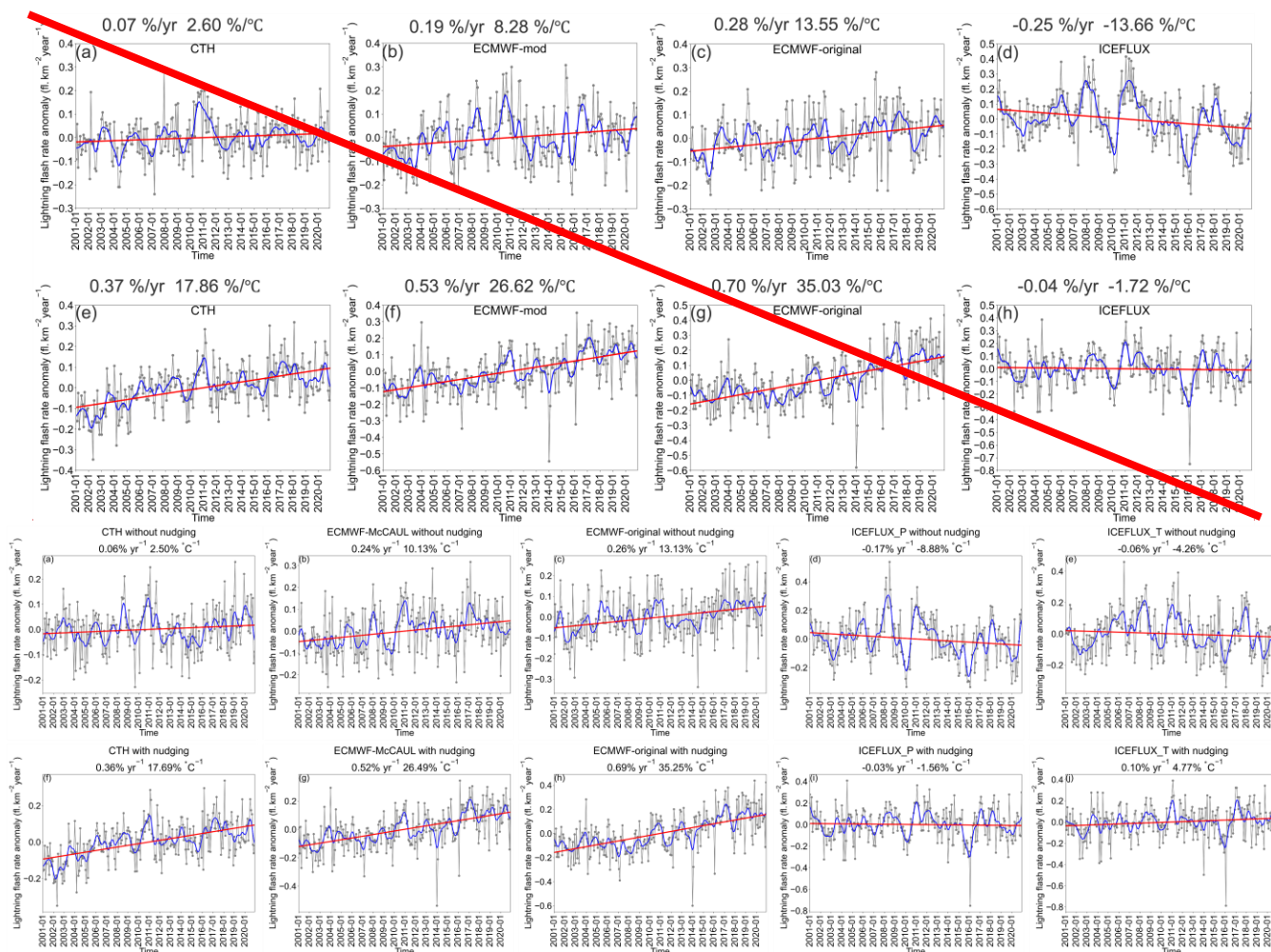
579

580 Figure 11: Effects of ECMWF-McCAUL scheme, original ECMWF scheme, and ICEFLUX_P scheme on the atmospheric chemical
 581 fields (NO_x, O₃, OH, CO) relative to the CTH scheme on the zonal mean (%).

582 3.4 Long-term Historical trend analysis of lightning density

583 The accuracy of predicting the simulated lightning distribution under the current climate is only one aspect of lightning
 584 scheme evaluation. The ability of the lightning scheme to reproduce the trend of lightning under climate change is also an
 585 important factor. For this study, 20 years of (2001–2020) experiments were conducted to analyze the long-term historical
 586 trends of lightning flash rates simulated using different lightning schemes (section Sect. 2.4).

587



588

589 **Figure 412: Global anomaly of lightning flash rates calculated from simulation results (2001–2020) using different lightning schemes.**
 590 **Figures 412(a–d) present results without nudging; Figs. 412(e–h) present results with nudging. The grey**
 591 **lines with points represent the monthly time-series data of the global mean lightning flash rate anomaly. The blue curves represent**
 592 **the monthly time-series data of the global mean lightning flash rate anomaly with the 1-D Gaussian (Denosing) Filter applied. The**
 593 **red lines are the fitting curves of the grey lines.**

595 **Table 4: Changes in global mean surface temperature (ΔTS), global mean lightning flash rate (ΔLFR), and the rate of change of**
 596 **lightning flash rate corresponding to each degree Celsius increase in global mean surface temperature ($\Delta LFR/\Delta TS$). The upper panel**
 597 **shows results obtained without nudging. The lower panel presents results obtained with nudging. Changes were obtained by**
 598 **calculating the difference between the rightmost and leftmost points of the approximating curve for the 2001–2020 time-series data.**

Lightning scheme	ΔTS (°C)	ΔLFR (%)	$\Delta LFR/\Delta TS$ (%/°C)
CTH	0.38	0.95	2.50
ECMWF-McCAUL	0.39	3.95	10.13
ECMWF-original	0.40	5.25	13.13
ICEFLUX_P	0.40	-3.55	-8.88
ICEFLUX_T	0.34	-1.45	-4.26

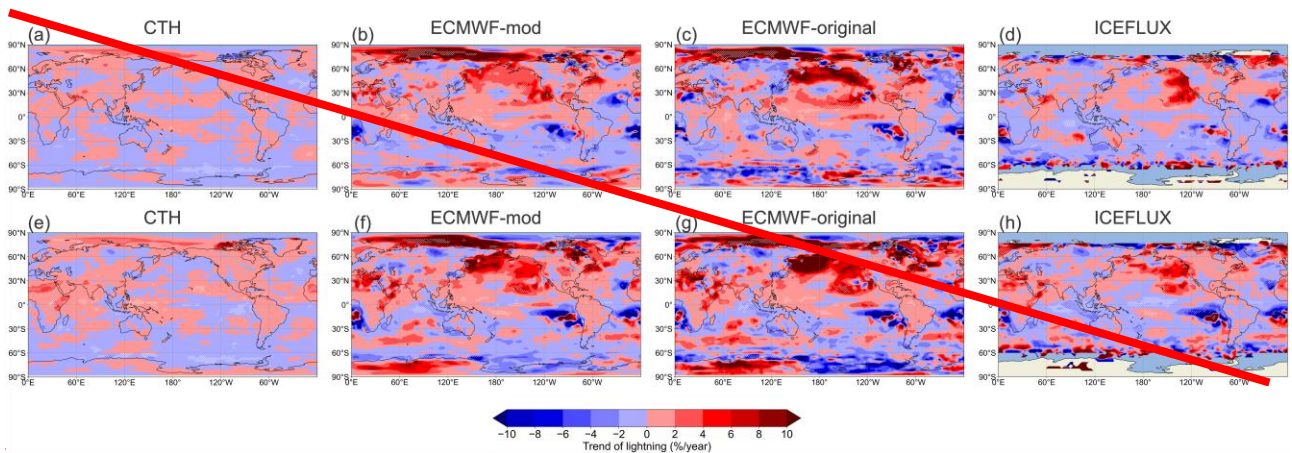
Lightning scheme	ΔTS (°C)	ΔLFR (%)	$\Delta LFR/\Delta TS$ (%/°C)
CTH	0.39	6.90	17.69
ECMWF-McCAUL	0.39	10.33	26.49
ECMWF-original	0.39	13.74	35.23
ICEFLUX_P	0.39	-0.61	-1.56
ICEFLUX_T	0.39	1.86	4.77

599

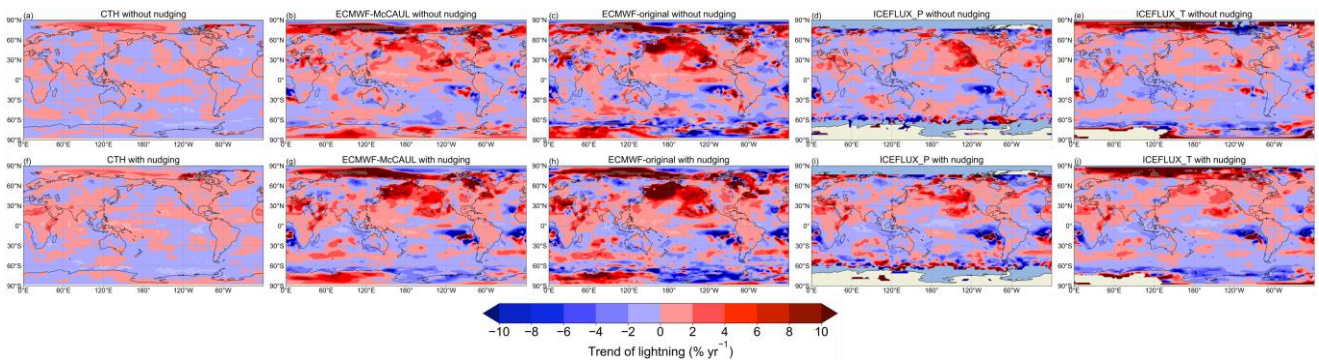
600 Figure 4+12 shows the global anomaly of lightning flash rates calculated from the simulation results. Because nudging to
 601 meteorological reanalysis data cannot be used when predicting lightning trends under future climate changes, we also
 602 showed the results without nudging. The un-nudged runs also represented the short-term surface warming like the
 603 experiments with nudging. The only differences between the un-nudged and nudged experiments are whether the
 604 meteorological fields are nudged towards the six-hourly NCEP FNL data. We used the Mann–Kendall rank statistic to
 605 ascertain whether the lightning trends in Fig. 4+12 are significant (Hussain et al., 2019). From results of the Mann–Kendall
 606 rank statistic test (significance set as 5%), all the trends in Fig. 4+12 were inferred as significant except for the case of the
 607 ICEFLUX scheme with nudging applied. trends shown in Figs. 12a, e, i. As Fig. 4+12 shows, all lightning schemes predicted
 608 increasing trends or no significant trends of lightning except the ICEFLUX_P scheme without nudging, which predicted a
 609 decreasing lightning trend. These results are consistent with those of earlier studies (Price and Rind, 1994; Zeng et al., 2008;
 610 Jiang and Liao, 2013; Banerjee et al., 2014; Krause et al., 2014; Clark et al., 2017; Finney et al., 2018), which reported that
 611 the CTH scheme predicted a 5%–16% increase of The isotherms alternative application of ICEFLUX (ICEFLUX_T) led to
 612 slightly enhanced lightning flashes per degree of increase in global mean surface temperatures and which reported that trends
 613 toward positive lighting trends compared to the ICEFLUX_P scheme. As explained by Romps (2019), the ICEFLUX_P
 614 approach is based on a fixed isobar which makes it inappropriate for climate change studies. Therefore, at least the
 615 ICEFLUX scheme predicted a 15% decrease of total lightning flash rate trends simulated by the ICEFLUX_T approach are
 616 expected closer to the real situation than the ICEFLUX_P approach.

617
 618 As displayed in 2100 under Representative Concentration Pathway 8.5 (RCP8.5). The Fig. 12, the positive lightning trends
 619 are generally enhanced by application of meteorological nudging. A further investigation of the trends of CAPE during
 620 2001–2020 discloses that the trends of global averaged CAPE are also enhanced by application of meteorological nudging.
 621 Since higher CAPE means higher buoyancy in the updrafts, which led to the higher lightning densities calculated by the
 622 lightning schemes used in this study. It is worth noting that even though the meteorological fields (u, v, T) of nudged
 623 simulations are expected closer to the real situations, we cannot analogously deduce that the lightning trends predicted by the
 624 nudged runs are also closer to the real situations. This is because the predicted lightning trends are not only controlled by the
 625 meteorological fields but also controlled by many other physical processes (e.g., cumulus parameterization).

626
 627 Few studies have specifically examined the lightning trends predicted by the ECMWF schemes under global the short-term
 628 surface warming. When nudging was not applied, the ECMWF schemes predicted the increasing trends of lightning flash
 629 rates under global the short-term surface warming by factors of 3 (modified 4 (ECMWF-McCAUL scheme) and 5 (original
 630 ECMWF scheme) compared to the CTH scheme (Table 4).



631

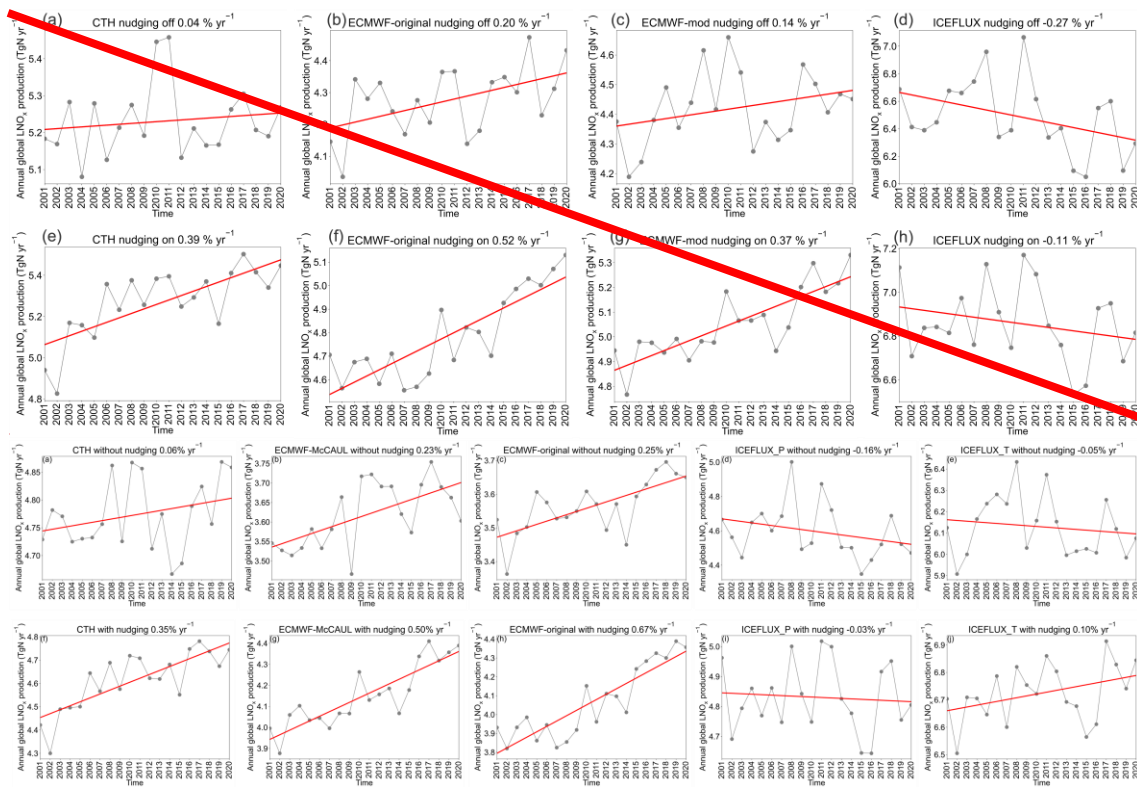


632
 633 **Figure 1213:** Changes in the lightning flash rate ($\% \text{ yr}^{-1}$) during 2001–2020 on the two-dimensional map. Changes at every point
 634 were calculated from the function of approximating curve for the 2001–2020 time-series data at each grid cell. Figures 1213(a–e)
 635 show results without nudging; Figs. 1213(f–l) show results with nudging. There are some missing values in the case of the
 636 ICEFLUX scheme because the upward cloud ice flux used is diagnosed as zero by the CHASER model typically within the high
 637 latitude regions.
 638

639 Figure 1213 shows a global map of changes in the lightning flash rate ($\% \text{ yr}^{-1}$) during 2001–2020. In Fig. 1213, the area in
 640 which the trend was found to be significant by the Mann–Kendall rank statistic test (significance level inferred for 5%) is
 641 marked with hatched lines. As Fig. 1213 shows, the distribution of trends simulated by the same lightning scheme is similar
 642 whether meteorological nudging was applied or not. As displayed in Fig. 1213, in the Arctic region of the Eastern
 643 Hemisphere, both the CTH scheme and the ECMWF schemes showed an increasing trend of lightning. Earlier studies based
 644 on the World Wide Lightning Location Network (WWLLN) lightning observations have indicated that lightning densities in
 645 the Arctic increase concomitantly with increasing global mean surface temperature (Holzworth et al., 2021). Earlier studies
 646 indicate that the results of the CTH scheme and the ECMWF schemes are reasonable for the Arctic region of the Eastern
 647 Hemisphere. In the high latitude region of the Southern Hemisphere (60°S – 70°S), both the CTH scheme and the ECMWF
 648 schemes showed decreasing lightning trends. Lightning is rarely observed south of 60°S (Kelley, et al., 2018). Moreover, the
 649 trends of lightning in this region expected to occur with global the short-term surface warming remain highly uncertain. In
 650 some parts of the Northern Pacific Ocean, the ECMWF schemes and ICEFLUX scheme results showed increasing trends of
 651 lightning, which is consistent with results obtained from an earlier study (Walter and Buechler, 2008). All schemes show
 652 decreasing trends for lightning flash rates in Indonesia, although only the ICEFLUX scheme explicitly passed the
 653 significance test. In the North Atlantic, all schemes showed increasing lightning trends. Only the CTH scheme failed the
 654 significance test.

655 3.5 Effects of LNO_x emissions on trends of tropospheric O₃ and NO_x columns

656 The long-term historical trends of lightning densities during 2001–2020 calculated using different lightning schemes have
 657 been discussed in section Sect. 3.4. Increasing or decreasing trends of lightning can engender corresponding trends of LNO_x
 658 emissions, which can consequently influence trends of NO_x and O₃ concentrations. To ascertain the extent to which the
 659 LNO_x emissions influence NO_x and O₃ concentration trends, the effects of the LNO_x emissions on the trends of tropospheric
 660 NO_x and O₃ columns have been estimated and discussed. We conducted two sets of experiments (section Sect. 2.4), one of
 661 which interactively calculated LNO_x emission rates, whereas the other one maintained the 2001 LNO_x emission rates for
 662 simulations of the entire 20 years. The LNO_x emission effects on the trends of tropospheric NO_x and O₃ columns can be
 663 estimated quantitatively by comparing the results of these two sets of experiments. We also conducted the verification of the
 664 simulated trends of tropospheric NO_x and O₃ columns by the OMI satellite observations and the results are exhibited in Fig.
 665 S1 and Fig. S2. Generally, the model has well captured the trends of global averaged tropospheric NO₂ and O₃ columns even
 666 though the trends of both tropospheric NO₂ and O₃ columns are underestimated by the model. Overall, it is obvious that the
 667 modelled trends with interannually varying LNO_x emissions with nudging are most close to the OMI observations.

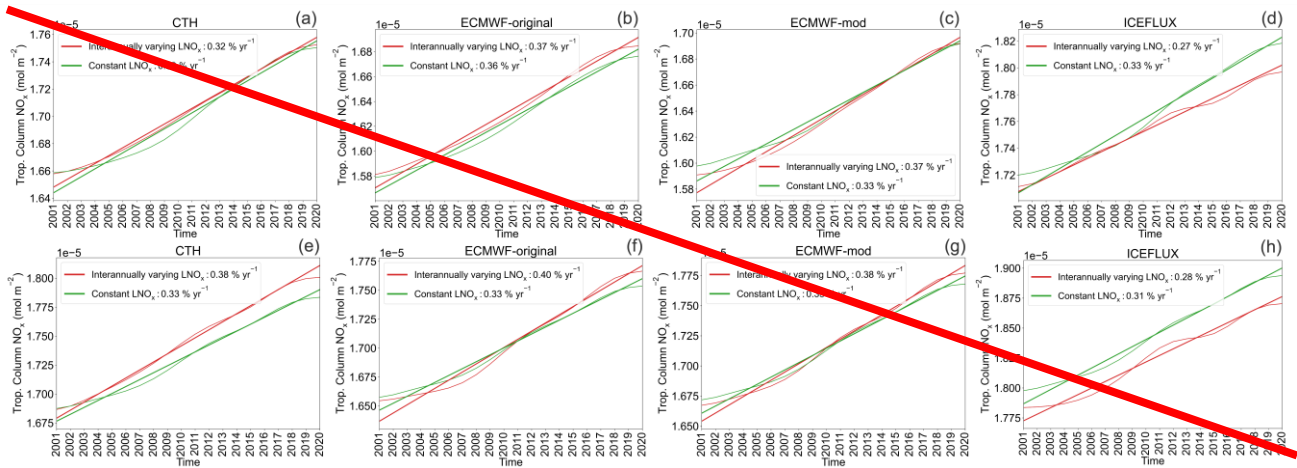


668

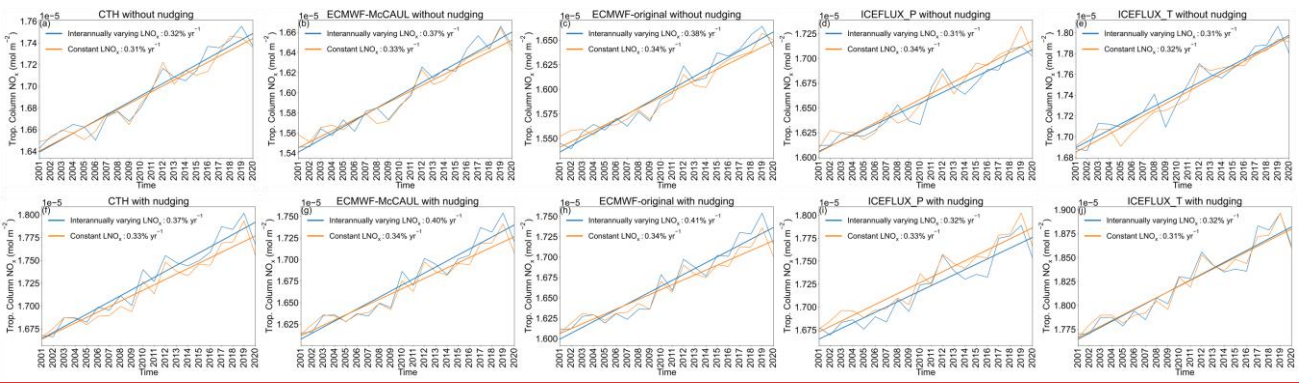
669

670 **Figure 13**: Trends of annual global LNO_x emissions calculated from simulation results (2001–2020) from different lightning
 671 schemes. Red lines are fitting curves. Figures 13(a–d) present results without nudging; Figs. 13(e–h) present results with
 672 nudging. The number in the title of each figure represents the trend corresponding to that figure in the unit of % yr⁻¹.
 673

674 Figure 13 presents trends of annual global LNO_x emissions calculated from the simulation results (2001–2020) obtained
 675 using different lightning schemes. As Fig. 13 shows, the annual global LNO_x emission trends correspond to the trends of
 676 lightning presented in Fig. 11. Similarly, similar to the trends found for lightning, the trends of annual global LNO_x
 677 emissions are also increased by application of meteorological nudging. Only the ICEFLUX scheme simulated decreasing
 678 trends of annual global LNO_x emissions.

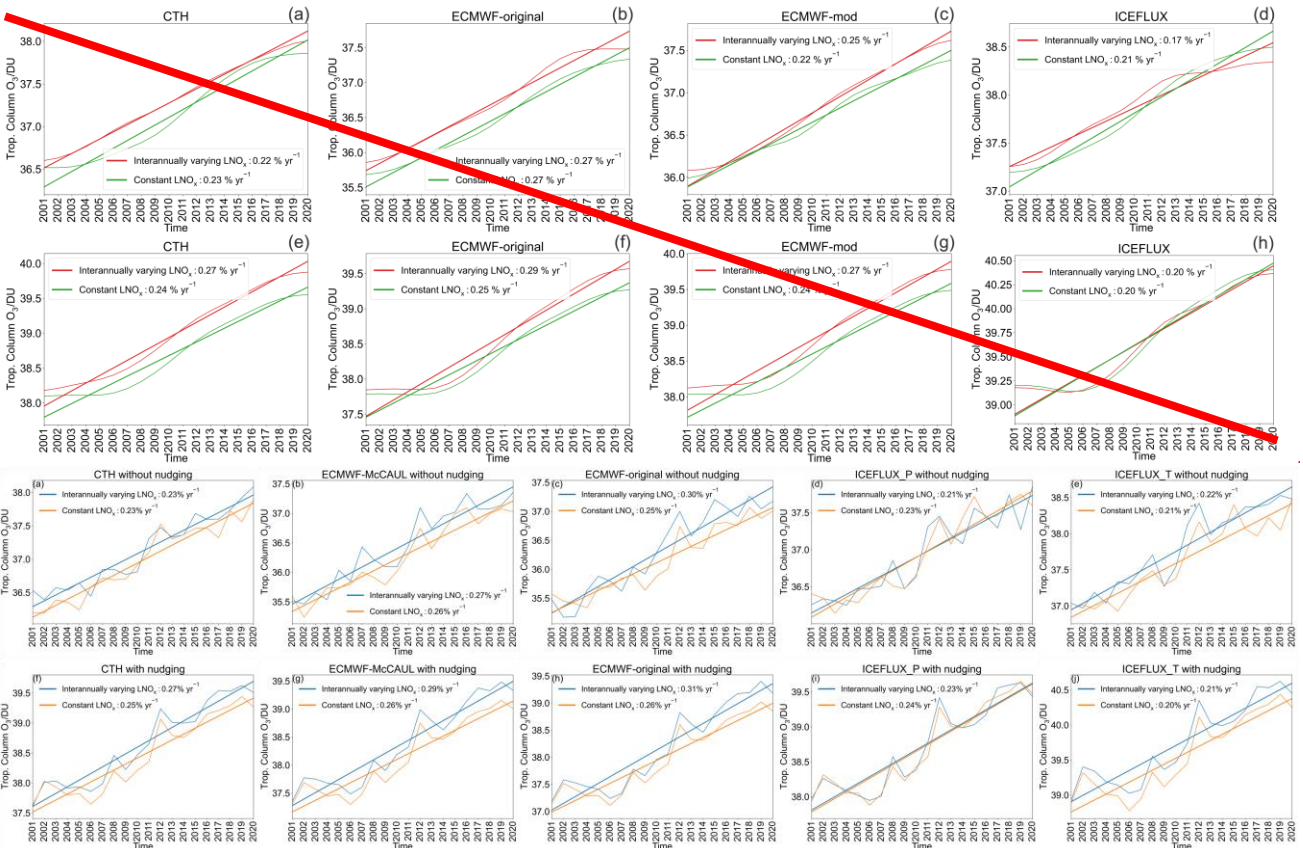


679



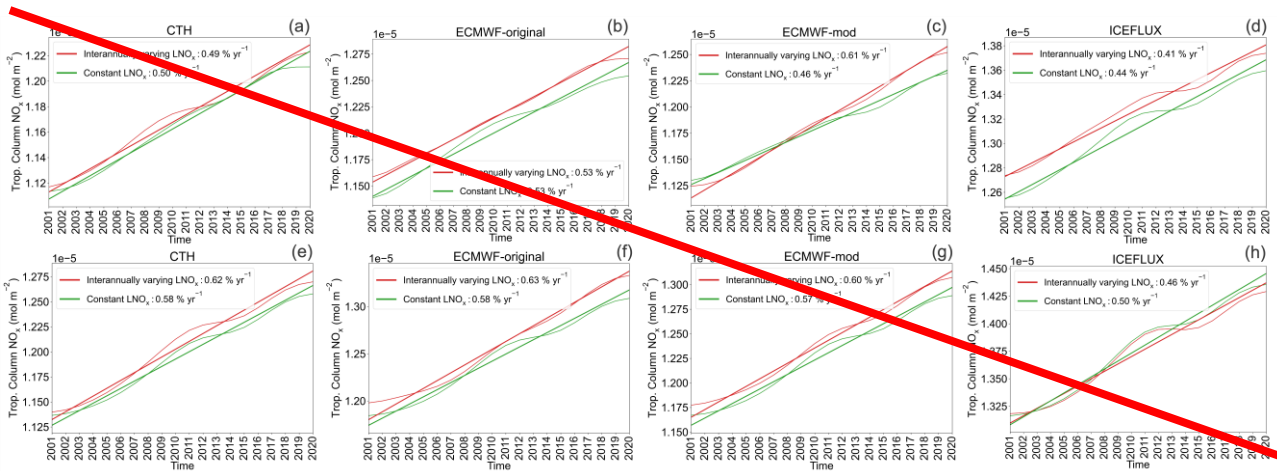
680
 681 **Figure 1415:** Trends of global mean tropospheric NO_x columns calculated from simulation results (2001–2020) using different
 682 lightning schemes. Straight lines in the figure are the fitting curves. **Straight lines and curves in red are results calculated using the**
 683 **first set of experiments. Straight lines and curves in green show results calculated using the second set of experiments (Table 2).** The
 684 numbers in legends represent trends corresponding to that figure in the unit of % yr⁻¹. Figures 1415(a–d) present results obtained
 685 without nudging; Figs. 1415(e–j) present results obtained with nudging.

687 Figure 1415 portrays trends of global mean tropospheric NO_x columns calculated from the first and second set of
 688 experiments (Table 2). As Fig. 1414 and Fig. 1415 depict, when the trends of annual global LNO_x emissions are not strong
 689 (e.g., Fig. 1414a), their effects on the trends of global mean tropospheric NO_x columns are negligible. The marked
 690 increasing trends of annual global LNO_x emissions (Figs. 1414e, 1414f, g, h) led to great increases (15.2%–21.2, 12%–
 691 20.59%) of the increasing trends of tropospheric NO_x columns (Figs. 1415e, 1415f, g, h). In the case of the ICEFLUX_P scheme
 692 without nudging, because of the decreasing trends of LNO_x emissions, the increasing trends of the tropospheric NO_x columns
 693 decreased by around 10%.

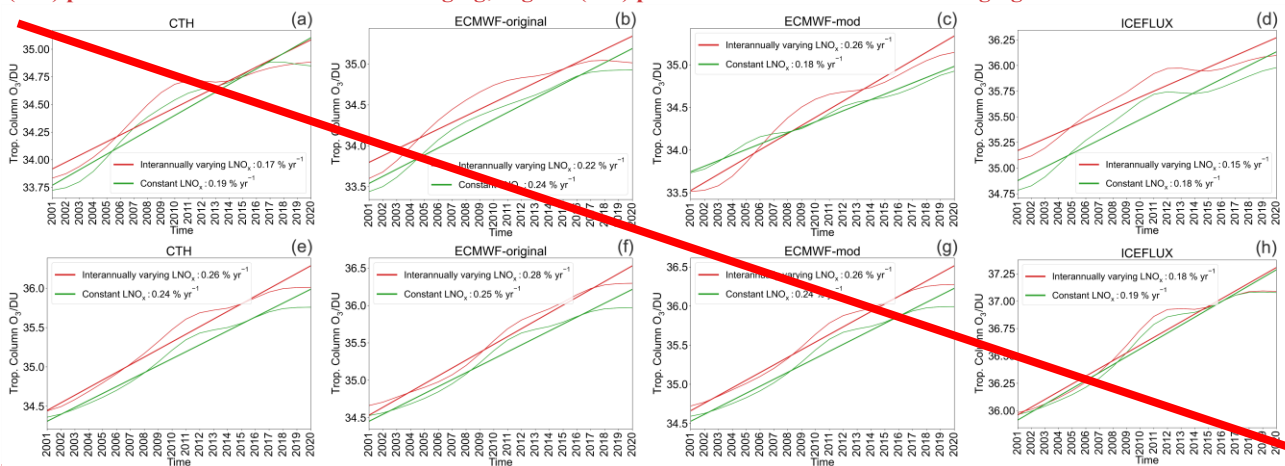


694
 695 **Figure 1516:** Trends of global mean tropospheric O₃ columns calculated from simulation results (2001–2020) using different lightning
 696 schemes. Straight lines in the figure are the fitting curves. **Straight lines and curves in red are results calculated using the first set of**
 697 **experiments. Straight lines and curves in green are results calculated using the second set of experiments (Table 2).** The number in
 698 the legend represents the trend corresponding to that figure in the unit of % yr⁻¹. Figures 1516(a–d) present results obtained without
 699 nudging; Figs. 1516(e–h) show results obtained with nudging.

702 Figure 1516 is similar to the results shown in Fig. 1415, but for tropospheric O₃ columns. Because NO_x causes the formation
 703 of O₃ by the fundamental chemical cycle of O_x-NO_x-HO_x, the trends of the global mean tropospheric O₃ columns are
 704 affected strongly by trends of the global mean tropospheric NO_x columns. For CTH and the original ECMWF schemes
 705 without nudging (Figs. 14a, b and Figs. 15a, b), in some cases, the simulated trends of tropospheric O₃ columns are almost
 706 identical as portrayed in Figs. 16 a, b, e, i, j because the trends of tropospheric NO_x columns simulated by the two sets of
 707 experiments are very similar. (Figs. 15 a, b, e, i, j). As Fig. 1314 and Fig. 1516 show, the marked increasing trends of annual
 708 global LNO_x emissions led to increases of the increasing trends of tropospheric O₃ columns by around 15% (Figs. 15e, 16f,
 709 g, h). In the case of ICEFLUX_P without nudging, because of the decreasing trend of LNO_x emissions, the increasing trend
 710 of the tropospheric O₃ columns decreased by around 20% (Fig. 15d), 10% (Fig. 16d). Note that the tropospheric NO_x or O₃
 711 columns in 2001 simulated by the first set of experiments and the second set of experiments are not exactly the same. This is
 712 because the blue lines show results with interactively calculated LNO_x emission rates (the time resolution is 10–30 minutes).
 713 But the orange lines show results calculated by reading daily mean input data for LNO_x emission rates, which inhibits
 714 interaction of LNO_x with meteorology in the model.



715 **Figure 16: Trends of North Pacific region (10°S–60°N; 150°E–240°E) mean tropospheric NO_x columns calculated from simulation**
 716 **results (2001–2020) by different lightning schemes. Straight lines in the figure are the fitting curves. Straight lines and curves in red**
 717 **are results calculated using the first set of experiments. Straight lines and curves in green are results calculated using the second**
 718 **set of experiments (Table 2). The number in the legend represents the trend corresponding to that figure in the unit of % yr⁻¹. Figures**
 719 **16(a–d) present results obtained without nudging; Figs. 16(e–h) present results obtained with nudging.**
 720



721 **Figure 17: Trends of North Pacific region (10°S–60°N; 150°E–240°E) mean tropospheric O₃ columns calculated from the simulation**
 722 **results (2001–2020) by different lightning schemes. Straight lines in the figure are the fitting curves. Straight lines and curves in red**
 723 **are the results calculated using the first set of experiments. Straight lines and curves in green are the results calculated using the**
 724 **second set of experiments (Table 2). The number in the legend represents the trend corresponding to that figure in the unit of % yr⁻¹.**
 725 **Figures 17(a–d) show the results obtained without nudging; Figs. 17(e–h) show the results obtained with nudging.**
 726

728 As discussed in Section 3.4, lightning densities increased or decreased to a considerable degree in different regions of the
 729 world, as simulated by all the introduced lightning schemes (Fig. 12). We chose to investigate the LNO_x emission effects on
 730 the tropospheric NO_x and O₃ column trends over a region with greatly increasing LNO_x, as simulated by the ECMWF

731 schemes (North Pacific region 10°S–60°N; 150°E–240°E). Figure 16 shows trends of North Pacific region (10°S–60°N;
732 150°E–240°E) mean tropospheric NO_x columns calculated from the first and second set of experiments (Table 2). Figure 17
733 is similar to the graphic presented in Fig. 16, but for tropospheric O₃ columns. In the case of the modified ECMWF scheme
734 without nudging (Fig. 16e and Fig. 17e), because of the increasing trend of LNO_x emissions, the trends of tropospheric NO_x
735 and O₃ columns increased significantly by 32.6% and 44.4%, respectively. However, although the LNO_x emissions increased
736 significantly in the case of the original ECMWF scheme without nudging, the trends simulated by the first and second set of
737 experiments are almost identical (Fig. 16b). This close approximation might be attributable to the different meteorological
738 conditions and chemical fields during simulations.

739

740 In conclusion, because the ICEFLUX scheme predicts the opposite trends of LNO_x emissions from the other lightning
741 schemes, they simulate opposite effects on the long-term historical trends of global mean tropospheric NO_x and O₃ columns.
742 Furthermore, an evident trend of annual global ~~(regional)~~ LNO_x emissions has a strong effect on the trend of global
743 ~~(regional)~~ mean tropospheric NO_x and O₃ columns.

744 **4 Discussions and Conclusions**

745 ~~Two~~Three new lightning schemes, the ICEFLUX ~~and~~ the original ECMWF ~~and the ECMWF-McCAUL~~ schemes, were
746 implemented into CHASER (MIROC), a global chemical climate model. ~~By modifying the equations and adjustment factors~~
747 ~~from the original ECMWF scheme based on work reported by McCaul et al. (2009), a new modified ECMWF scheme was~~
748 ~~also tested with CHASER (MIROC).~~

749

750 Using LIS/OTD lightning observations as validation data, both the ICEFLUX P and ECMWF schemes simulated the spatial
751 distribution of lightning more accurately on a global scale than the CTH scheme did, and the lightning distribution in the
752 ocean region was especially improved. The ~~modified~~ ECMWF-McCAUL scheme showed the highest prediction accuracy
753 for the spatial distribution of lightning on a global scale. It is noteworthy that whilst the ice-based parametrisations showed
754 superb prediction accuracy of lightning distribution under today's climate, they have greater uncertainties associated with
755 inputs, especially regarding the microphysics scheme used (Charn and Parishani, 2021).

756

757 To verify the LNO_x emissions of different lightning schemes, we used NO observations from ATom1 and ATom2. Overall,
758 both the ICEFLUX P scheme and the ECMWF schemes partially reduced ~~the~~ model biases typically over the dominant
759 regions of lightning activities compared to the CTH scheme, ~~except in the case of comparison between the modified~~
760 ~~ECMWF scheme and ATom2 observations. Although both the ICEFLUX scheme and the ECMWF schemes reduced the~~
761 ~~model biases, the ICEFLUX scheme reduced the biases to a greater degree. Comparison of the model results with ATom1~~
762 ~~observations revealed that the ICEFLUX scheme has the lowest model biases at 30°S–80°N, whereas the CTH scheme has~~
763 ~~the lowest model biases at 30°S–80°S. When comparing the model outputs with ATom2 observations, the ICEFLUX scheme~~
764 ~~has the smallest model biases at low latitude region (30°S–30°N). Results show that the CTH scheme has the smallest model~~
765 ~~biases at middle latitude to high latitude regions.~~

766

767 We also used TROPOMI NO₂-tropospheric NO₂ columns to verify the LNO_x emissions of different lightning schemes.
768 Compared with the CTH scheme, the ICEFLUX scheme reduced theAlthough the ICEFLUX P and the ECMWF schemes
769 have not shown improvements of model biases of tropospheric NO₂ columns at an annual global mean model bias, whereas
770 the ECMWF schemes increased the global mean model bias, which indicates that the ICEFLUX scheme improved the LNO_x
771 simulation accuracy in the model. In the four target scale, they generally led to an obvious reduction of model biases in the

772 ~~prevailing seasons of lightning within the~~ regions where LNO_x is ~~the~~ dominant source of NO_x, ~~the ICEFLUX scheme is the~~
773 ~~best lightning scheme able to capture the seasonal variation of NO₂, whereas the ECMWF schemes only significantly~~
774 ~~improved the temporal correlations between the model and the~~. Several studies have pointed out that ~~the TROPOMI~~
775 ~~observations data used in this study biased negatively compared to the airborne or ground-based observation data (Tack et al.,~~
776 ~~2021; Verhoelst et al., 2021; van Geffen et al., 2022). Since the TROPOMI data used are generally negatively biased and the~~
777 ~~simulated tropospheric NO₂ columns are underestimated compared to the TROPOMI observations. Therefore, the~~
778 ~~uncertainties that existed in the Amazon region, TROPOMI data have negligible impacts on the conclusions of our study.~~

779

780 Effects of the newly implemented lightning schemes on the tropospheric chemical fields are evaluated compared to the CTH
781 scheme. Compared with the CTH scheme, the ECMWF schemes mainly led to a slight increase in NO_x, ozone, and OH
782 radical concentrations at low latitude regions and a decrease at middle-latitude to high-latitude regions. Effects of the
783 ICEFLUX P scheme on the tropospheric chemical fields slightly differ from those of the ECMWF schemes. The ICEFLUX
784 ~~model P scheme~~ mainly causes a slight increase of NO_x, ozone, and OH radical concentrations ~~in from the tropics to~~ the
785 Northern Hemisphere and a decrease in the concentrations of the three chemical species in the Southern Hemisphere.
786 ~~Commonality except the tropics. The commonality~~ between the ECMWF schemes and the ICEFLUX P scheme is that they
787 both result in decreasing concentrations of NO_x, ozone, and OH radical at the middle to high latitude regions of the Southern
788 Hemisphere. Although the newly implemented lightning schemes have little effect on the total oxidation capacity of the
789 troposphere compared to the CTH scheme, they led to marked ~~changechanges~~ of oxidation capacity in different regions of
790 the atmosphere.

791

792 This study also analyzed the ~~long-term historical~~ trends of lightning simulated by different lightning schemes under ~~global the~~
793 ~~short-term surface~~ warming during 2001–2020. ~~All the lightning schemes predicted increasing lightning trends except the~~
794 ~~ICEFLUX scheme, which predicted a decreasing lightning trend.~~ The Mann–Kendall rank statistic was used to ascertain
795 whether the lightning trends were significant. Use of Mann–Kendall rank statistic tests revealed that all the ~~lightning trends~~
796 ~~are significant, except the ICEFLUX scheme with nudging applied, for significance at 5%.~~ simulated historical lightning
797 ~~trends are significant, except the CTH and the ICEFLUX T schemes without nudging and the ICEFLUX P scheme with~~
798 ~~nudging, for significance at 5%. All the lightning schemes predicted increasing lightning trends or no significant trends~~
799 ~~except the ICEFLUX P scheme without nudging, which predicted a decreasing lightning trend. The ICEFLUX T scheme~~
800 ~~predicted a decreasing trend without nudging even though the trend failed the significant test. If it's accepted that the non-~~
801 ~~inductive charging mechanism is an appropriate basis for a lightning parametrisation, then the implication is that in the~~
802 ~~future if cloud ice (and cloud ice fluxes) reduce then electrical charging will reduce too. This provides a line of scientific~~
803 ~~reasoning to explain why lightning may reduce in the future.~~ Moreover, findings showed that when nudging was not applied,
804 the ECMWF schemes predicted an increasing trend of lightning flash rate under ~~global the short-term surface~~ warming by
805 factors of ~~3 (modified 4~~ (ECMWF-McCAUL scheme) and 5 (original ECMWF scheme) compared to the CTH scheme.

806

807 ~~Finally, we quantitatively estimated the LNO_x emission effects on tropospheric NO_x and O₃ column trends during 2001–~~
808 ~~2020. Results showed that a marked trend of annual global (regional) LNO_x emissions significantly affects the trend of~~
809 ~~global (regional) mean tropospheric NO_x and O₃ columns.~~

810

811 ~~In summary, comparison with results obtained using the CTH scheme demonstrated that both the ICEFLUX and ECMWF~~
812 ~~schemes improved the prediction accuracy of the lightning distribution on a global scale. In fact, the modified ECMWF~~
813 ~~scheme has the highest prediction accuracy. Using ATom aircraft observations and TROPOMI satellite observations to~~
814 ~~verify the LNO_x emissions, the results show that, compared to the CTH scheme, the ICEFLUX scheme reduced the model~~

815 ~~biases to a greater degree than the ECMWF schemes.~~ Although a considerable degree of uncertainty remains in ~~the~~
816 ~~prediction of lightning trends under global warming, results of most studies have indicated that the global~~determining the
817 ~~sensitivity of lightning activity to changes in surface temperature on the decadal timescale (Williams 2005), the majority of~~
818 ~~past estimates show the sensitivity tends~~ average lightning density can be expected to increase by about close to 10% for
819 ~~each degree of global warming~~ K^{-1} (Betz et al., 2008, p. 521). This value is most consistent with the lightning increase rate
820 predicted by the ~~modified~~-ECMWF-McCAUL scheme without nudging in this study. Future research should be undertaken
821 for specific examination of development of lightning schemes that both accurately predict the global distribution of LNO_x
822 and which predict the changes in lightning that are expected to occur concomitantly with global climate change. Finally, we
823 quantitatively estimated the LNO_x emission effects on tropospheric NO_x and O₃ column trends during 2001–2020. Results
824 showed that a marked trend of annual global LNO_x emissions significantly affects the trend of global mean tropospheric NO_x
825 and O₃ columns.

826 Code availability

827 The source code for CHASER to reproduce results in this work is obtainable from the repository at
828 <https://doi.org/10.5281/zenodo.5835796> (He et al., 2022)

829 Data availability

830 The LIS/OTD data used for this study are available from <https://ghrc.nsstc.nasa.gov/hydro/?q=LRTS> (last access: 11 January
831 2022). The ATom data used for this study are available from https://daac.ornl.gov/ATOM/guides/ATom_merge.html (last
832 access: 11 January 2022). The TROPOMI data used for this study are available from
833 <https://s5phub.copernicus.eu/dhus/#/home> (last access: 11 January 2022). The OMI level-3 daily global gridded (0.25° ×
834 0.25°) Nitrogen Dioxide product (OMNO2d) used for this study is available from
835 https://disc.gsfc.nasa.gov/datasets/OMNO2d_003/summary (last access: 25 May 2022). The OMI/MSL tropospheric column
836 ozone data used for this study are available from https://acd-ext.gsfc.nasa.gov/Data_services/cloud_slice/new_data.html (last
837 access: 25 May 2022).

838 Author contribution

839 YFH introduced new lightning schemes into CHASER (MIROC) by adding new codes to CHASER (MIROC), conducted all
840 simulations, interpreted the results, and wrote the manuscript. KS developed the model code, conceived of the presented
841 idea, and supervised the findings of this work and the manuscript preparation. HMSH provided the TROPOMI data and the
842 relevant codes to pre-process the TROPOMI data.

843 Competing interests

844 The authors declare that they have no conflict of interest.

845 Acknowledgements

846 This research was supported by the Global Environment Research Fund (S–12 and S–20) of the Ministry of the Environment
847 (MOE), Japan, and JSPS KAKENHI Grant Numbers: JP20H04320, JP19H05669, and JP19H04235. This work was
848 supported by Japan Science and Technology Agency (JST) Support for Pioneering Research Initiated by the Next Generation
849 (SPRING), Grant Number JPMJSP2125. The author (Initial) would like to take this opportunity to thank the
850 “Interdisciplinary Frontier Next-Generation Researcher Program of the Tokai Higher Education and Research System.” The
851 simulations were completed with the supercomputer (NEC SX-Aurora TSUBASA) at NIES (Japan). Thanks to NASA
852 scientists and staff for providing LIS/OTD lightning observation data
853 (https://ghrc.nsstc.nasa.gov/uso/ds_docs/lis_climatology/LISOTD_climatology_dataset.html, last access: 9 January 2022)
854 ~~and~~, ATom data (<https://espo.nasa.gov/atom/content/ATom>, last access: 9 January 2022~~),~~ and OMI satellite observation
855 data (https://disc.gsfc.nasa.gov/datasets/OMNO2d_003/summary, last access: 25 May 2022; [https://acd-](https://acd-ext.gsfc.nasa.gov/Data_services/cloud_slice/new_data.html)
856 [ext.gsfc.nasa.gov/Data_services/cloud_slice/new_data.html](https://acd-ext.gsfc.nasa.gov/Data_services/cloud_slice/new_data.html), last access: 25 May 2022). We are grateful to ESA scientists

857 and staff for providing TROPOMI data (<http://www.tropomi.eu>, last access: 9 January 2022). We thank Yannick Copin for
858 software he developed to help us with the Taylor diagram.

859 **References**

860 [Allen, D. J., Pickering, K. E., Bucsele, E., Krotkov, N., and Holzworth, R.: Lightning NO_x Production in the Tropics as](#)
861 [Determined Using OMI NO₂ Retrievals and WWLLN Stroke Data, *J. Geophys. Res. Atmos.*, 124, 13498–13518,](#)
862 <https://doi.org/10.1029/2018JD029824>, 2019.

863
864 Banerjee, A., Archibald, A. T., Maycock, A. C., Telford, P., Abraham, N. L., Yang, X., Braesicke, P., and Pyle, J. A.:
865 Lightning NO_x, a key chemistry-climate interaction: impacts of future climate change and consequences for tropospheric
866 oxidising capacity, *Atmos. Chem. Phys.*, 14, 9871–9881, <https://doi.org/10.5194/acp-14-9871-2014>, 2014.

867
868 Betz, H. D., Schumann, U., and Laroche, P.: *Lightning: Principles, instruments and applications: Review of modern*
869 *lightning research*, Springer Netherlands, 1–641 pp., <https://doi.org/10.1007/978-1-4020-9079-0>, 2009.

870
871 [Boccippio, Dennis J., William J. Koshak, and Richard J. Blakeslee.: Performance Assessment of the Optical Transient](#)
872 [Detector and Lightning Imaging Sensor. Part I: Predicted Diurnal Variability, *Journal of Atmospheric and Oceanic*](#)
873 [Technology](#), 19, 1318-1332, [https://doi.org/10.1175/1520-0426\(2002\)019<1318:PAOTOT>2.0.CO;2](https://doi.org/10.1175/1520-0426(2002)019<1318:PAOTOT>2.0.CO;2), 2002

874
875 [Bucsele, E. J., Pickering, K. E., Allen, D. J., Holzworth, R. H., and Krotkov, N. A.: Midlatitude Lightning NO_x Production](#)
876 [Efficiency Inferred From OMI and WWLLN Data, *J. Geophys. Res. Atmos.*, 124, 13475–13497,](#)
877 <https://doi.org/10.1029/2019JD030561>, 2019.

878
879 Cecil, D. J., Buechler, D. E., and Blakeslee, R. J.: Gridded lightning climatology from TRMM-LIS and OTD: Dataset
880 description, *Atmos. Res.*, 135–136, 404–414, <https://doi.org/10.1016/j.atmosres.2012.06.028>, 2014.

881
882 [Charn, A. B. and Parishani, H.: Predictive Proxies of Present and Future Lightning in a Superparameterized Model, *J.*](#)
883 [Geophys. Res. Atmos., 126, e2021JD035461, <https://doi.org/10.1029/2021JD035461>, 2021.](#)

884
885 Clark, S. K., Ward, D. S., and Mahowald, N. M.: Parameterization-based uncertainty in future lightning flash density,
886 *Geophys. Res. Lett.*, 44, 2893–2901, <https://doi.org/10.1002/2017GL073017>, 2017.

887
888 [Cooray, V., Rahman, M., and Rakov, V.: On the NO_x production by laboratory electrical discharges and lightning, *J. Atmos.*](#)
889 [Solar-Terrestrial Phys., 71, 1877–1889, <https://doi.org/10.1016/j.jastp.2009.07.009>, 2009.](#)

890
891 Finney, D. L., Doherty, R. M., Wild, O., Huntrieser, H., Pumphrey, H. C., and Blyth, A. M.: Using cloud ice flux to
892 parametrise large-scale lightning, *Atmos. Chem. Phys.*, 14, 12665–12682, <https://doi.org/10.5194/acp-14-12665-2014>, 2014.

893
894 Finney, D. L., Doherty, R. M., Wild, O., Young, P. J., and Butler, A.: Response of lightning NO_x emissions and ozone
895 production to climate change: Insights from the Atmospheric Chemistry and Climate Model Intercomparison Project,
896 *Geophys. Res. Lett.*, 43, 5492–5500, <https://doi.org/10.1002/2016GL068825>, 2016a.

897
898 Finney, D. L., Doherty, R. M., Wild, O., and Abraham, N. L.: The impact of lightning on tropospheric ozone chemistry using
899 a new global lightning parametrisation, *Atmos. Chem. Phys.*, 16, 7507–7522, <https://doi.org/10.5194/acp-16-7507-2016>,
900 2016b.

901

902 Finney, D. L., Doherty, R. M., Wild, O., Stevenson, D. S., MacKenzie, I. A., and Blyth, A. M.: A projected decrease in
903 lightning under climate change, *Nat. Clim. Chang.*, 8, 210–213, <https://doi.org/10.1038/s41558-018-0072-6>, 2018.

904

905 [Finney, D. L., Marsham, J. H., Wilkinson, J. M., Field, P. R., Blyth, A. M., Jackson, L. S., Kendon, E. J., Tucker, S. O., and](#)
906 [Stratton, R. A.: African Lightning and its Relation to Rainfall and Climate Change in a Convection-Permitting Model, 47,](#)
907 [e2020GL088163, <https://doi.org/10.1029/2020GL088163>, 2020.](#)

908

909 [Goldberg, D. L., Saide, P. E., Lamsal, L. N., De Foy, B., Lu, Z., Woo, J. H., Kim, Y., Kim, J., Gao, M., Carmichael, G., and](#)
910 [Streets, D. G.: A top-down assessment using OMI NO₂ suggests an underestimate in the NO_x emissions inventory in Seoul,](#)
911 [South Korea, during KORUS-AQ, *Atmos. Chem. Phys.*, 19, 1801–1818, <https://doi.org/10.5194/acp-19-1801-2019>, 2019.](#)

912

913 Grewe, V.: Impact of climate variability on tropospheric ozone, *Sci. Total Environ.*, 374, 167–181,
914 <https://doi.org/10.1016/j.scitotenv.2007.01.032>, 2007.

915

916 Ha, P. T. M., Matsuda, R., Kanaya, Y., Taketani, F., and Sudo, K.: Effects of heterogeneous reactions on tropospheric
917 chemistry: A global simulation with the chemistry-climate model CHASER V4.0, *Geosci. Model Dev.*, 14, 3813–3841,
918 <https://doi.org/10.5194/gmd-14-3813-2021>, 2021.

919

920 He, Y., Hoque, M. S. H., and Sudo, K.: Introducing new lightning schemes into the CHASER (MIROC) chemistry climate
921 model [Code], Zenodo, <https://doi.org/10.5281/ZENODO.5835796>, 2022.

922

923 [Heath, N. K., Pleim, J. E., Gilliam, R. C., and Kang, D.: A simple lightning assimilation technique for improving](#)
924 [retrospective WRF simulations, 8, 1806–1824, <https://doi.org/10.1002/2016MS000735>, 2016.](#)

925

926 Holzworth, R. H., Brundell, J. B., McCarthy, M. P., Jacobson, A. R., Rodger, C. J., and Anderson, T. S.: Lightning in the
927 Arctic, *Geophys. Res. Lett.*, 48, e2020GL091366, <https://doi.org/10.1029/2020GL091366>, 2021.

928

929 Hui, J. and Hong, L.: Projected Changes in NO_x Emissions from Lightning as a Result of 2000–2050 Climate Change,
930 *Atmos. Ocean. Sci. Lett.*, 6, 284–289, <https://doi.org/10.3878/j.issn.1674-2834.13.0042>, 2013.

931

932 Hussain, M. and Mahmud, I.: pyMannKendall: a python package for non parametric Mann Kendall family of trend tests., *J.*
933 *Open Source Softw.*, 4, 1556, <https://doi.org/10.21105/joss.01556>, 2019.

934

935 Inness, A., Baier, F., Benedetti, A., Bouarar, I., Chabrillat, S., Clark, H., Clerbaux, C., Coheur, P., Engelen, R. J., Errera, Q.,
936 Flemming, J., George, M., Granier, C., Hadji-Lazaro, J., Huijnen, V., Hurtmans, D., Jones, L., Kaiser, J. W., Kapsomenakis,
937 J., Lefever, K., Leitão, J., Razinger, M., Richter, A., Schultz, M. G., Simmons, A. J., Suttie, M., Stein, O., Thépaut, J.-N.,
938 Thouret, V., Vrekoussis, M., Zerefos, C., and the MACC team: The MACC reanalysis: an 8 yr data set of atmospheric
939 composition, *Atmos. Chem. Phys.*, 13, 4073–4109, <https://doi.org/10.5194/acp-13-4073-2013>, 2013.

940

941 Isaksen, I. S. A. and Hov, Ø.: Calculation of trends in the tropospheric concentration of O₃, OH, CO, CH₄ and NO_x, *Tellus B*,
942 39 B, 271–285, <https://doi.org/10.1111/j.1600-0889.1987.tb00099.x>, 1987.

943

944 [Kang, D., Foley, K. M., Mathur, R., Roselle, S. J., Pickering, K. E., and Allen, D. J.: Simulating lightning NO production in](#)
945 [CMAQv5.2: Performance evaluations, Geosci. Model Dev., 12, 4409–4424, <https://doi.org/10.5194/GMD-12-4409-2019>,](#)
946 [2019a.](#)

947

948 [Kang, D., Mathur, R., Pouliot, G. A., Gilliam, R. C., and Wong, D. C.: Significant ground-level ozone attributed to](#)
949 [lightning-induced nitrogen oxides during summertime over the Mountain West States, npj Clim. Atmos. Sci. 2020 31, 3, 1–](#)
950 [7, <https://doi.org/10.1038/s41612-020-0108-2>, 2020.](#)

951

952 [Kang, D., Pickering, K. E., Allen, D. J., Foley, K. M., Wong, D. C., Mathur, R., and Roselle, S. J.: Simulating lightning NO](#)
953 [production in CMAQv5.2: evolution of scientific updates, Geosci. Model Dev., 12, 3071–3083,](#)
954 [https://doi.org/10.5194/GMD-12-3071-2019, 2019b.](#)

955

956 Kelley, O. A., Thomas, J. N., Solorzano, N. N., and Holzworth, R. H.: Fire and Ice: Intense ~~convective~~convective
957 precipitation observed at high latitudes by the GPM satellite’s Dual-frequency Precipitation Radar (DPR) and the ground-
958 based World Wide Lightning Location Network (WWLLN), AGU Poster, 2018, H43F-2487, 2018.

959

960 Krause, A., Kloster, S., Wilkenskjeld, S., and Paeth, H.: The sensitivity of global wildfires to simulated past, present, and
961 future lightning frequency, J. Geophys. Res. Biogeosciences, 119, 312–322, <https://doi.org/10.1002/2013JG002502>, 2014.

962

963 Labrador, L. J., von Kuhlmann, R., and Lawrence, M. G.: The effects of lightning-produced NO_x and its vertical distribution
964 on atmospheric chemistry: sensitivity simulations with MATCH-MPIC, Atmos. Chem. Phys., 5, 1815–1834,
965 <https://doi.org/10.5194/acp-5-1815-2005>, 2005.

966

967 Lamarque, J. F., Shindell, D. T., Josse, B., Young, P. J., Cionni, I., Eyring, V., Bergmann, D., Cameron-Smith, P., Collins,
968 W. J., Doherty, R., Dalsoren, S., Faluvegi, G., Folberth, G., Ghan, S. J., Horowitz, L. W., Lee, Y. H., MacKenzie, I. A.,
969 Nagashima, T., Naik, V., Plummer, D., Righi, M., Rumbold, S. T., Schulz, M., Skeie, R. B., Stevenson, D. S., Strode, S.,
970 Sudo, K., Szopa, S., Voulgarakis, A., and Zeng, G.: The atmospheric chemistry and climate model intercomparison Project
971 (ACCMIP): Overview and description of models, simulations and climate diagnostics, Geosci. Model Dev., 6, 179–206,
972 <https://doi.org/10.5194/gmd-6-179-2013>, 2013.

973

974 Liaskos, C. E., Allen, D. J., and Pickering, K. E.: Sensitivity of tropical tropospheric composition to lightning NO_x
975 production as determined by replay simulations with GEOS-5, J. Geophys. Res., 120, 8512–8534,
976 <https://doi.org/10.1002/2014JD022987>, 2015.

977

978 Lopez, P.: A lightning parameterization for the ECMWF integrated forecasting system, Mon. Weather Rev., 144, 3057–
979 3075, <https://doi.org/10.1175/MWR-D-16-0026.1>, 2016.

980

981 McCaul, E. W., Goodman, S. J., LaCasse, K. M., and Cecil, D. J.: Forecasting lightning threat using cloud-resolving model
982 simulations, Weather Forecast., 24, 709–729, <https://doi.org/10.1175/2008WAF2222152.1>, 2009.

983

984 Murray, L. T.: Lightning NO_x and Impacts on Air Quality, <https://doi.org/10.1007/s40726-016-0031-7>, 25 April 2016.

985

986 [Nickolay A. Krotkov, Lok N. Lamsal, Sergey V. Marchenko, Edward A. Celarier, Eric J. Bucsele, William H. Swartz, Joanna](#)
987 [Joiner and the OMI core team: OMI/Aura NO₂ Cloud-Screened Total and Tropospheric Column L3 Global Gridded 0.25](#)
988 [degree × 0.25 degree V3, Goddard Earth Sciences Data and Information Services Center \(GES DISC\) \[data set\],](#)
989 [10.5067/Aura/OMI/DATA3007, 2019](#)
990

991 Ott, L. E., Pickering, K. E., Stenchikov, G. L., Allen, D. J., DeCaria, A. J., Ridley, B., Lin, R. F., Lang, S., and Tao, W. K.:
992 Production of lightning NO_x and its vertical distribution calculated from three-dimensional cloud-scale chemical transport
993 model simulations, *J. Geophys. Res. Atmos.*, 115, D04301, <https://doi.org/10.1029/2009JD011880>, 2010.
994

995 Pickering, K. E., Wang, Y., Tao, W. K., Price, C., and Müller, J. F.: Vertical distributions of lightning NO_x for use in
996 regional and global chemical transport models, *J. Geophys. Res. Atmos.*, 103, 31203–31216,
997 <https://doi.org/10.1029/98JD02651>, 1998.
998

999 Price, C. and Rind, D.: A simple lightning parameterization for calculating global lightning distributions, *J. Geophys. Res.*,
1000 97, 9919–9933, <https://doi.org/10.1029/92JD00719>, 1992.
1001

1002 Price, C. and Rind, D.: What determines the cloud-to-ground lightning fraction in thunderstorms?, *Geophys. Res. Lett.*, 20,
1003 463–466, <https://doi.org/10.1029/93GL00226>, 1993.
1004

1005 Price, C. and Rind, D.: Possible implications of global climate change on global lightning distributions and frequencies, *J.*
1006 *Geophys. Res.*, 99, 823–833, <https://doi.org/10.1029/94jd00019>, 1994.
1007

1008 ~~Price~~Rayner, N. A., Parker, D. E., Horton, E. B., Folland, C., Penner, J. K., Alexander, L. V., Rowell, D. P., Kent, E. C., and
1009 Prather, M.: NO_x from lightning 1. Kaplan, A.: Global distribution based on lightning physics, J. analyses of sea surface
1010 temperature, sea ice, and night marine air temperature since the late nineteenth century, 108 ~~Geophys. Res. Atmos.~~, 102,
1011 ~~5929–5941~~, <https://doi.org/10.1029/96jd03504>, 1997 ~~2002JD002670~~, 2003.
1012

1013 [Ridley, B. A., Pickering, K. E., and Dye, J. E.: Comments on the parameterization of lightning-produced NO in global](#)
1014 [chemistry-transport models, *Atmos. Environ.*, 39, 6184–6187, <https://doi.org/10.1016/j.atmosenv.2005.06.054>, 2005.](#)
1015

1016 Romps, D. M.: Evaluating the Future of Lightning in Cloud-Resolving Models, *Geophys. Res. Lett.*, 46, 14863–14871,
1017 <https://doi.org/10.1029/2019GL085748>, 2019.
1018

1019 Romps, D. M., Seeley, J. T., Vollaro, D., and Molinari, J.: Projected increase in lightning strikes in the united states due to
1020 global warming, *Science* (80-.), 346, 851–854, <https://doi.org/10.1126/science.1259100>, 2014.
1021

1022 Schumann, U. and Huntrieser, H.: The global lightning-induced nitrogen oxides source, *Atmos. Chem. Phys.*, 7, 3823–3907,
1023 <https://doi.org/10.5194/acp-7-3823-2007>, 2007.
1024

1025 Sudo, K. and Akimoto, H.: Global source attribution of tropospheric ozone: Long-range transport from various source
1026 regions, 112, <https://doi.org/10.1029/2006JD007992>, 2007.
1027

1028 Sudo, K., Takahashi, M., Kurokawa, J. I., and Akimoto, H.: CHASER: A global chemical model of the troposphere 1. Model
1029 description, *J. Geophys. Res. Atmos.*, 107, ACH 7-1-ACH 7-20, <https://doi.org/10.1029/2001JD001113>, 2002.

1030

1031 [Tack, F., Merlaud, A., Iordache, M. D., Pinardi, G., Dimitropoulou, E., Eskes, H., Bomans, B., Veefkind, P., and Van](#)
1032 [Roosendael, M.: Assessment of the TROPOMI tropospheric NO₂ product based on airborne APEX observations, *Atmos.*](#)
1033 [Meas. Tech.](#), 14, 615–646, <https://doi.org/10.5194/amt-14-615-2021>, 2021.

1034

1035 Takemura, T., Egashira, M., Matsuzawa, K., Ichijo, H., O’Ishi, R., and Abe-Ouchi, A.: A simulation of the global
1036 distribution and radiative forcing of soil dust aerosols at the Last Glacial Maximum, *Atmos. Chem. Phys.*, 9, 3061–3073,
1037 <https://doi.org/10.5194/acp-9-3061-2009>, 2009.

1038

1039 [Thornhill, G., Collins, W., Olivié, D., B. Skeie, R., Archibald, A., Bauer, S., Checa-Garcia, R., Fiedler, S., Folberth, G.,](#)
1040 [Gjermundsen, A., Horowitz, L., Lamarque, J. F., Michou, M., Mulcahy, J., Nabat, P., Naik, V., M. O’Connor, F., Paulot, F.,](#)
1041 [Schulz, M., E. Scott, C., Séférian, R., Smith, C., Takemura, T., Tilmes, S., Tsigaridis, K., and Weber, J.: Climate-driven](#)
1042 [chemistry and aerosol feedbacks in CMIP6 Earth system models, *Atmos. Chem. Phys.*, 21, 1105–1126,](#)
1043 <https://doi.org/10.5194/acp-21-1105-2021>, 2021.

1044

1045 Tost, H.: Chemistry–climate interactions of aerosol nitrate from lightning, *Atmos. Chem. Phys.*, 17, 1125–1142,
1046 <https://doi.org/10.5194/acp-17-1125-2017>, 2017.

1047

1048 Tost, H., Jöckel, P., and Lelieveld, J.: Lightning and convection parameterisations – Uncertainties in global modelling,
1049 *Atmos. Chem. Phys.*, 7, 4553–4568, <https://doi.org/10.5194/acp-7-4553-2007>, 2007.

1050

1051 [van Geffen, J., Eskes, H., Compernelle, S., Pinardi, G., Verhoelst, T., Lambert, J.-C., Sneep, M., ter Linden, M., Ludewig,](#)
1052 [A., Boersma, K. F., and Veefkind, J. P.: Sentinel-5P TROPOMI NO₂ retrieval: impact of version v2.2 improvements and](#)
1053 [comparisons with OMI and ground-based data, *Atmos. Meas. Tech.*, 15, 2037–2060, \[2022, 2022.\]\(https://doi.org/10.5194/amt-15-2037-
1054 <a href=\)](#)

1055

1056 [Verhoelst, T., Compernelle, S., Pinardi, G., Lambert, J. C., Eskes, H. J., Eichmann, K. U., Fjæraa, A. M., Granville, J.,](#)
1057 [Niemeijer, S., Cede, A., Tiefengraber, M., Hendrick, F., Pazmiño, A., Bais, A., Bazureau, A., Folkert Boersma, K., Bognar,](#)
1058 [K., Dehn, A., Donner, S., Elokhov, A., Gebetsberger, M., Goutail, F., Grutter De La Mora, M., Gruzdev, A., Gratsea, M.,](#)
1059 [Hansen, G. H., Irie, H., Jepsen, N., Kanaya, Y., Karagkiozidis, D., Kivi, R., Kreher, K., Levelt, P. F., Liu, C., Müller, M.,](#)
1060 [Navarro Comas, M., PETERS, A. J. M., Pommereau, J. P., Portafaix, T., Prados-Roman, C., Puentedura, O., Querel, R.,](#)
1061 [Remmers, J., Richter, A., Rimmer, J., Cárdenas, C. R., De Miguel, L. S., Sinyakov, V. P., Stremme, W., Strong, K., Van](#)
1062 [Roosendael, M., Pepijn Veefkind, J., Wagner, T., Wittrock, F., Yela González, M., and Zehner, C.: Ground-based validation](#)
1063 [of the Copernicus Sentinel-5P TROPOMI NO₂ measurements with the NDACC ZSL-DOAS, MAX-DOAS and Pandonia](#)
1064 [global networks, *Atmos. Meas. Tech.*, 14, 481–510, <https://doi.org/10.5194/amt-14-481-2021>, 2021.](#)

1065

1066 Walter A. Petersen and D. Buechler: Global tropical lightning trends: Has tropical lightning frequency responded to global
1067 climate change?, in: Third Conference on Meteorological Applications of Lightning Data, New Orleans, USA, 20-28
1068 January 2008, 2.1, 2008

1069

1070 Watanabe, S., Hajima, T., Sudo, K., Nagashima, T., Takemura, T., Okajima, H., Nozawa, T., Kawase, H., Abe, M.,
1071 Yokohata, T., Ise, T., Sato, H., Kato, E., Takata, K., Emori, S., and Kawamiya, M.: MIROC-ESM 2010: Model description
1072 and basic results of CMIP5-20c3m experiments, *Geosci. Model Dev.*, 4, 845–872, <https://doi.org/10.5194/gmd-4-845-2011>,
1073 2011.

1074

1075 Wild, O.: Modelling the global tropospheric ozone budget: Exploring the variability in current models, *Atmos. Chem. Phys.*,
1076 7, 2643–2660, <https://doi.org/10.5194/acp-7-2643-2007>, 2007.

1077

1078 [Williams, E. R.: Lightning and climate: A review, *Atmos. Res.*, 76, 272–287,](https://doi.org/10.1016/j.atmosres.2004.11.014)
1079 <https://doi.org/10.1016/j.atmosres.2004.11.014>, 2005.

1080

1081 Wofsy, S. C., Afshar, S., Allen, H. M., Apel, E., Asher, E. C., Barletta, B., Bent, J., Bian, H., Biggs, B. C., Blake, D. R.,
1082 Blake, N., Bourgeois, I., Brock, C. A., Brune, W. H., Budney, J. W., Bui, T. P., Butler, A., Campuzano-Jost, P., Chang, C.
1083 S., Chin, M., Commane, R., Correa, G., Crouse, J. D., Cullis, P. D., Daube, B. C., Day, D. A., Dean-Day, J. M., Dibb, J. E.,
1084 Digangi, J. P., Diskin, G. S., Dollner, M., Elkins, J. W., Erdesz, F., Fiore, A. M., Flynn, C. M., Froyd, K., Gesler, D. W.,
1085 Hall, S. R., Hanisco, T. F., Hannun, R. A., Hills, A. J., Hints, E. J., Hoffman, A., Hornbrook, R. S., Huey, L. G., Hughes, S.,
1086 Jimenez, J. L., Johnson, B. J., Katich, J. M., Keeling, R., Kim, M. J., Kupc, A., Lait, L. R., Lamarque, J. F., Liu, J., McKain,
1087 K., McLaughlin, R. J., Meinardi, S., Miller, D. O., Montzka, S. A., Moore, F. L., Morgan, E. J., Murphy, D. M., Murray, L.
1088 T., Nault, B. A., Neuman, J. A., Newman, P. A., Nicely, J. M., Pan, X., Paplawsky, W., Peischl, J., Prather, M. J., Price, D.
1089 J., Ray, E., Reeves, J. M., Richardson, M., Rollins, A. W., Rosenlof, K. H., Ryerson, T. B., Scheuer, E., Schill, G. P.,
1090 Schroder, J. C., Schwarz, J. P., St. Clair, J. M., Steenrod, S. D., Stephens, B. B., Strode, S. A., Sweeney, C., Tanner, D.,
1091 Teng, A. P., Thames, A. B., Thompson, C. R., Ullmann, K., Veres, P. R., Vizenor, N., Wagner, N. L., Watt, A., Weber, R.,
1092 Weinzierl, B., Wennberg, P., Williamson, C J, Wilson, J C, Wolfe, G M, Woods, C T, Zeng, L H: ATom: Merged
1093 Atmospheric Chemistry, Trace Gases, and Aerosols, <https://doi.org/10.3334/ornlDaac/1581>, 2018.

1094

1095 [Yienger, J. J. and Levy, H.: Empirical model of global soil-biogenic NO_x emissions, *J. Geophys. Res.*, 100,](https://doi.org/10.1029/95jd00370)
1096 <https://doi.org/10.1029/95jd00370>, 1995.

1097

1098 Zeng, G., Pyle, J. A., and Young, P. J.: Impact of climate change on tropospheric ozone and its global budgets, *Atmos.*
1099 *Chem. Phys.*, 8, 369–387, <https://doi.org/10.5194/acp-8-369-2008>, 2008.

1100

1101 [Ziemke, J. R., Chandra, S., Duncan, B. N., Froidevaux, L., Bhartia, P. K., Levelt, P. F., and Waters, J. W.: Tropospheric](https://doi.org/10.1029/2006JD007089)
1102 [ozone determined from Aura OMI and MLS: Evaluation of measurements and comparison with the Global Modeling](https://doi.org/10.1029/2006JD007089)
1103 [Initiative's Chemical Transport Model, 111, 19303, https://doi.org/10.1029/2006JD007089](https://doi.org/10.1029/2006JD007089), 2006.